RESEARCH ARTICLE

Key Points:
- Magmatism caused by lithosphere removal is studied with geodynamic models
- Five types of magmatism in different tectonic settings are identified
- Magmas reveal removal mechanisms in the central Andes and Sierra Nevada

Correspondence to:
H. Wang,
huilin1@ualberta.ca

Magmatic expressions of continental lithosphere removal

Huilin Wang[1,2] and Claire A. Currie[1]

[1]Department of Physics, University of Alberta, Edmonton, Alberta, Canada, [2]Now at Seismological Laboratory, California Institute of Technology, Pasadena, California, USA

Abstract Gravitational lithosphere removal in continental interior has been inferred from various observations, including anomalous surface deflections and magmatism. We use numerical models and a simplified theoretical analysis to investigate how lithosphere removal can be recognized in the magmatic record. One style of removal is a Rayleigh-Taylor-type instability, where removal occurs through dripping. The associated magmatism depends on the lithosphere thermal structure. Four types of magmatism are predicted: (1) For relatively hot lithosphere (e.g., back arcs), the lithosphere can be conductively heated and melted during removal, while the asthenosphere upwells and undergoes decompression melting. If removal causes significant lithospheric thinning, the deep crust may be heated and melted. (2) For moderately warm lithosphere (e.g., average Phanerozoic lithosphere) in which the lithosphere root has a low density, only the lithosphere may melt. (3) If the lithosphere root has a high density in moderately warm lithosphere, only asthenosphere melt is predicted. (4) For cold lithosphere (e.g., cratons), no magmatism is induced. An alternate style of removal is delamination, where dense lithosphere peels along Moho. In most cases, the lithosphere sinks too rapidly to melt. However, asthenosphere can upwell to the base of the crust, resulting in asthenospheric and crustal melts. In delamination, magmatism migrates laterally with the detachment point; in contrast, magmatism in Rayleigh-Taylor-type instability has a symmetric shape and converges toward the drip center. The models may explain the diversity of magmatism observed in areas with inferred lithosphere removal, including the Puna Plateau and the southern Sierra Nevada.

1. Introduction

Gravitational lithosphere removal appears to have occurred in a number of continental regions, causing magmatism that is sourced from both the mantle and crust. A range of geophysical and geochemical observations supports the idea that a significant portion of continental lithosphere has been recycled into the deeper mantle. For example, seismic images show that the mantle lithosphere is thin and the asthenosphere is located less than 20 km below the crust in regions such as the Altiplano-Puna plateau in South America [*Myers et al.*, 1998; *Bianchi et al.*, 2012; *Heit et al.*, 2014], the western North Island in New Zealand [*Stern et al.*, 2006; *Salmon et al.*, 2013], and the Wallowa Mountains in Oregon [*Hales et al.*, 2005; *Darold and Humphreys*, 2013]. These observations conflict with the expectation that felsic crust should be underlain by a thick ultramafic/mafic root in order to balance geochemical element budgets [*Rudnick and Fountain*, 1995; *Plank*, 2005; *Lee et al.*, 2006]. Furthermore, seismic studies find small-scale (50–100 km wide) high-velocity anomalies in the shallow sublithospheric mantle (100–200 km depth) of the southern Sierra Nevada and the Great Basin in the United States [*West et al.*, 2009; *Saleeby et al.*, 2012], the western Mediterranean in southern Spain and northern Morocco [*Thurner et al.*, 2014], and the Puna plateau [*Schurr et al.*, 2006; *Bianchi et al.*, 2012]. These are interpreted as pieces of lithosphere that have detached from the overlying plate.

Seismic observations provide snapshots of present-day lithosphere removal events. Ongoing and ancient removal events may be traced through anomalous surface observations, including the generation of local basins/orogens, crustal contraction/extension, and increased heat flow and magmatism [e.g., *Springer*, 1999; *Farmer et al.*, 2002; *Gao et al.*, 2008; *Göğüş and Pysklywec*, 2008; *DeCelles et al.*, 2015; *Schoenbohm and Carrapa*, 2015]. Magmatism is usually considered the clearest evidence, as it indicates a rapid thermal change in the deep lithosphere [*Kay and Kay*, 1993]. Magmas provide temperature and compositional information of their source region, and therefore, they can be used to investigate the mechanism and scale of lithosphere recycling [e.g., *Kay et al.*, 1994; *Ducea*, 2011]. However, a comparison of regions with inferred removal events shows that the magma source composition and pressure-temperature (PT) evolution can be variable. In addition, some intracratonic basins appear to be linked with lithosphere removal, but there is no associated magmatism [*Elkins-Tanton*, 2005].

The classical view is that magmatism originates from decompression melting of asthenospheric mantle that upwells to replace the removed lithosphere [e.g., *Kay and Kay*, 1993; *Kay et al.*, 1994]. In this case, the rising asthenosphere follows a mantle adiabat and its melting temperature and pressure should decrease over time [*Kay et al.*, 1994]. For example, the southern Sierra Nevada experienced an eruption of high-potassium mafic magmas in the Pliocene. These are interpreted to reflect decompression melting of metasomatized asthenosphere following lithosphere foundering [e.g., *Ducea and Saleeby*, 1996, 1998; *Manley et al.*, 2000; *Farmer et al.*, 2002; *Elkins-Tanton and Grove*, 2003].

The foundering lithosphere may also contribute to the magmatism. *Elkins-Tanton* [2005, 2007] suggests that devolatilization of the descending lithosphere may trigger melting of the surrounding asthenosphere. In addition, conductive heating of the foundering lithosphere may result in melting of this material. *Ducea et al.* [2013] and *Murray et al.* [2015] find that the composition of young magmas (ages <5 Ma) in the southern Puna plateau has changed over time. The earliest magmatism appears to have been extracted from lithospheric pyroxentites, whereas more recent magma is consistent with an asthenospheric peridotite source. The melting temperature of lithospheric pyroxenites increased from ~1200°C to ~1300°C over a ~1 Myr timescale [*Ducea et al.*, 2013]. This trend is contrary to the expected temperature decrease for decompression melting. They hypothesize that the magmatism is related to lithospheric foundering; initial melts were generated by conductive heating and melting of small pieces of sinking lithosphere, whereas later melts originated from the upwelling asthenosphere.

The expressions of magmatism are further complicated if the remaining lithosphere (lithospheric mantle and/or crust) experiences partial melting owing to rapid heating following a removal event. This has been proposed to explain silicic volcanism in the southern Sierra Nevada [*Moore and Dodge*, 1980], shoshonitic volcanism in the Tibetan plateau [*Turner et al.*, 1993, 1996; *Chung et al.*, 2003], and felsic ignimbrites in the central Andes [*Schilling et al.*, 2006].

Most inferences of magmatism induced by lithosphere removal are based on geochemical observations. Only a few geodynamic studies have investigated magmatism. *Elkins-Tanton* [2005, 2007] studied melting associated with lithosphere removal as a Rayleigh-Taylor (RT) instability, in order to understand how asthenospheric melting may be induced by adiabatic upwelling and devolatilization of the descending lithosphere. *Gorczyk and Vogt* [2013] examined lithosphere dynamics during regional shortening and found that lithosphere removal and magmatism could occur under some conditions, depending on the preexisting structure of the lithosphere.

It is still not well understood how the magmatic signature of lithosphere removal may vary depending on the tectonic setting and removal style. In this study, thermal-mechanical models are used to study the magmatism and other surface expressions of removal, for settings ranging from a hot, thin lithosphere (i.e., back arc or mobile belt) to thick, cool lithosphere (i.e., stable continental interior). We then use a theoretical analysis of gravitational instability to extend the models to other conditions. Through this, we demonstrate the first-order controls on mantle-derived magmatism induced by lithosphere removal.

2. Mechanisms of Lithosphere Removal

Lithosphere removal is driven by gravitational instability of high-density lithosphere. The high density may be a result of thermal contraction, as the lithosphere is cooler than the underlying mantle [e.g., *Houseman and Molnar*, 1997]. Removal may also be triggered by a compositional difference between the lithosphere and underlying mantle [e.g., *Jull and Kelemen*, 2001]. Recent studies have focused on the role of pyroxenite [e.g., *DeCelles et al.*, 2009; *Ducea et al.*, 2013]. Pyroxenite can be generated from the cumulates and/or residues of ancient magmas [*Lee et al.*, 2006, 2011]. Garnet pyroxenite (loosely termed eclogite) [*Lee et al.*, 2006, 2011] is found within the garnet stability field at depths >40 km [*Rapp and Watson*, 1995], and it can be 50–250 kg/m^3 more dense than the peridotite mantle [e.g., *Ducea and Saleeby*, 1998; *Jull and Kelemen*, 2001; *Horodyskyj et al.*, 2007]. A xenolith study shows that a garnet pyroxenite root, which was ~40 km thick and 200 kg/m^3 denser than asthenospheric peridotite, existed beneath the central Sierra Nevada before the Pliocene removal event [*Ducea and Saleeby*, 1998]. A link between pyroxenite and lithosphere removal is further supported by magmatic evidence, which shows a pyroxenite magma source in several regions with inferred removal events, including the Puna plateau [*Ducea et al.*, 2013; *Murray et al.*, 2015] and the North China Craton [*Gao et al.*, 2008]. The solidus of pyroxenite is ~150°C lower than that of peridotite [*Hirschmann and Stolper*, 1996; *Pertermann and Hirschmann*, 2003; *Lambart et al.*, 2009]. Therefore, a lithosphere containing pyroxenite is more likely to melt as it descends into the hot asthenosphere.

There are two end-member styles of removal of high-density material. Lithosphere may be removed as a viscous Rayleigh-Taylor-type (RT) instability, in which the lithosphere descends symmetrically into the deep mantle as a "drip" [e.g., *Houseman and Molnar*, 1997]. This type of removal can be triggered by a lateral variation in density, such as a perturbation in lithosphere thickness due to shortening [e.g., *Molnar et al.*, 1998] or a localized high-density body [e.g., *Wang et al.*, 2015]. The other end-member is delamination, in which the lower lithosphere peels away from the upper plate as an intact layer along a weak interface [e.g., *Bird*, 1979; *Burov and Watts*, 2006]. A weak interface can form in the deep crust under a range of conditions, including high Moho temperatures [e.g., *Morency and Doin*, 2004] and metamorphic eclogitization of lower crust during lithosphere shortening [e.g., *Kay and Kay*, 1993; *Krystopowicz and Currie*, 2013; *Gorczyk et al.*, 2015]. In delamination, the lower lithosphere is removed asymmetrically as a coherent "plate-like" slice, whereas RT instability involves internal viscous deformation of the unstable lithosphere [e.g., *Göğüş and Pysklywec*, 2008]. It should be noted that there are intermediate styles of lithosphere removal. For example, at a sharp transition in lithosphere thickness, edge-driven convection may cause asymmetric viscous removal of the thicker lithosphere [e.g., *van Wijk et al.*, 2010; *Stern et al.*, 2013].

3. Numerical Methods

3.1. Modeling Approach

We address the magmatism that may be associated with the two end-member styles of lithosphere removal: RT instability and delamination. We first use two-dimensional numerical models to demonstrate the temporal evolution of magmatism generated by removal. The thermal-mechanical models use the finite element code SOPALE, which calculates the coupled thermal-mechanical evolution of the lithosphere-upper mantle system based on arbitrary Eulerian-Lagrangian techniques, assuming incompressibility and plane strain [*Fullsack*, 1995]. All models are 400 km deep and 800 km wide (Figure 1). The Eulerian mesh has 321×111 elements, with an element width of 2.5 km for the entire model domain. The element height is 2.5 km in the top 35 km, 1.25 km between 35 and 120 km depth, and 10 km at greater depths. The smaller elements ensure that the sinking lithosphere and upwelling asthenosphere are well resolved.

The models have a 40 km crust which overlies mantle lithosphere and asthenosphere. As shown below, the resulting magmatism depends on the initial lithosphere thickness and thermal structure. In section 4, we present models for two contrasting thermal structures (Figure 1). The first is a hot, thin lithosphere (75 km thick; 979°C Moho), which approximates a tectonically active region, such as a continental back arc [*Currie and Hyndman*, 2006]. The second has a cooler, thicker lithosphere (115 km thick, 610°C Moho). This is comparable to average Phanerozoic continental lithosphere and is somewhat warmer than a stable cratonic region [e.g., *Jaupart and Mareschal*, 1999].

To initiate removal, a high-density body, representing a pyroxenite "root," is placed in the mantle lithosphere immediately below the crust. The root is 15 km thick in the thin lithosphere model (Figure 1a) and 75 km thick in the model with thicker lithosphere (Figure 1b). This thickness is based on the maximum depth that pyroxenite is below its solidus for each model (i.e., the intersection between the lithosphere geotherm and pyroxenite solidus; Figure 1). This allows us to investigate melting that is generated during removal. The root is 200 km wide and 100 kg/m^3 denser than the underlying mantle, consistent with the density contrast between pyroxenite and peridotite [e.g., *Jull and Kelemen*, 2001]. Variations in root density, thickness, and width are considered in section 4.1.2.

For each lithosphere thickness, we model root removal through RT-type instability (dripping) and delamination. For RT-style removal, the presence of the dense root is sufficient to initiate instability; for delamination, a viscously weak zone is needed to facilitate detachment [e.g., *Göğüş and Pysklywec*, 2008]. In nature, delamination likely occurs at the Moho [e.g., *Bird*, 1979]. Therefore, in our delamination model, a weak layer with a constant viscosity of 10^{19} Pa s is placed at the right side of the root and along its surface at the Moho (Figure 1). The weak layer has the same density as the root material.

Table 1 gives the material parameters in the models, and Table 2 lists all models presented in this study. All materials have a viscous-plastic rheology and temperature-dependent density. At stresses above the frictional-plastic yield stress, materials follow a Drucker-Prager yield criterion, based on the effective internal
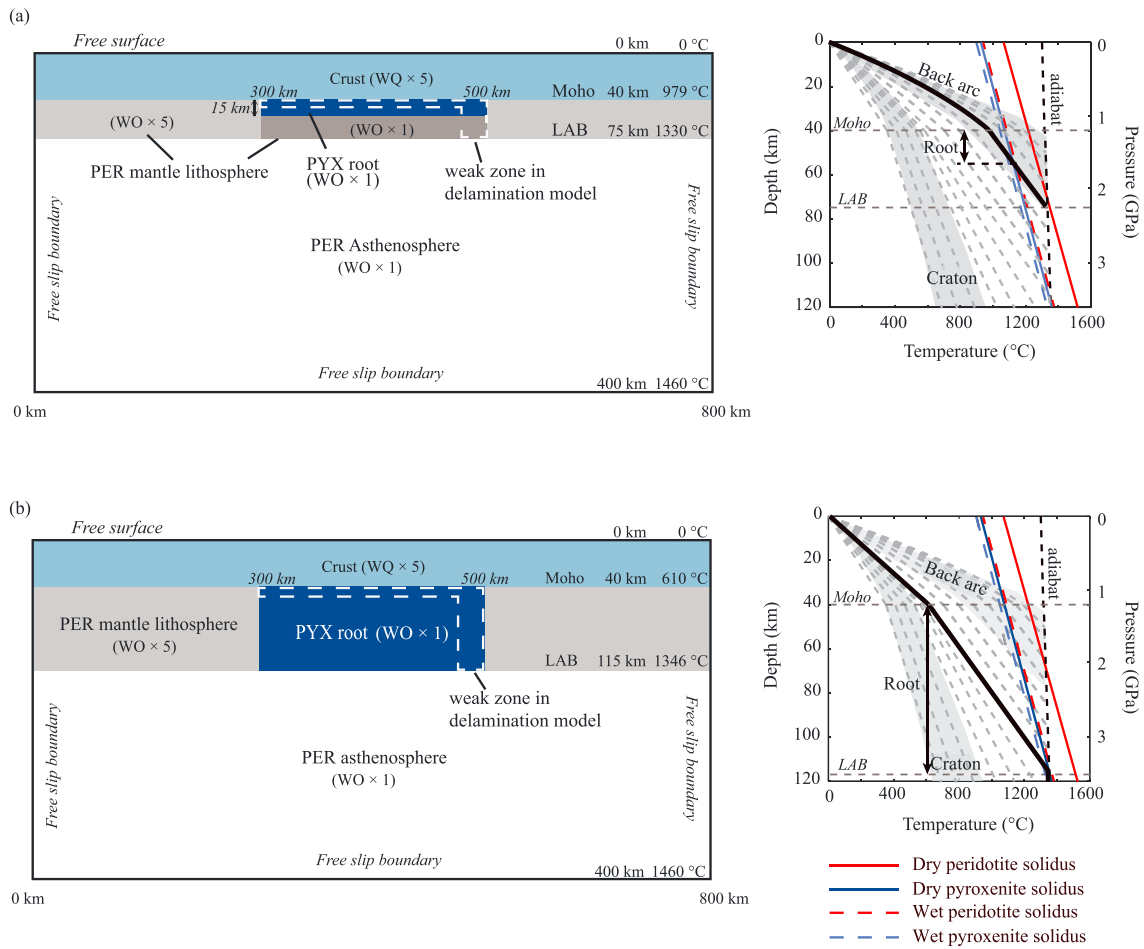
Figure 1. Numerical model setup for (a) a 75 km thick lithosphere and (b) a 115 km thick lithosphere. The delamination models include a weak zone with a viscosity of 10^{19} Pa s and density equal to that of the pyroxenite root (dashed white lines). For each thickness, the corresponding geotherm is shown in the right panel (solid black line), with the wet and dry solidus lines for peridotite (PER) and pyroxenite (PYX). The wet solidus corresponds to a water content of 5% H_2O for peridotite and 1% H_2O for pyroxenite. The dashed grey lines show the range of continental geotherms considered in section 5.2; the shaded regions show the thermal conditions for stable continental regions (cratons) and tectonically active regions (back arcs) [*Currie and Hyndman*, 2006]. LAB = lithosphere-asthenosphere boundary; WQ = wet quartzite; WO = wet olivine.

angle of friction (ϕ_{eff}) and cohesion (c_0) of each material [*Fullsack*, 1995]. At lower stresses, deformation occurs through viscous creep:

$$\eta_{eff}^{v} = f(B^*)(\dot{I}_2')^{\frac{1-n}{n}} \exp\left(\frac{Q + PV^*}{nRT_K}\right) \qquad (1)$$

where η_{eff}^{v} is the effective viscosity, $\dot{I}_2'^2$ is the second invariant of the strain rate tensor $\dot{\varepsilon}_{ij}$ ($\dot{I}_2'^2 = \frac{1}{2}\dot{\varepsilon}_{ij}\dot{\varepsilon}_{ij}$), R is the gas constant, and T_K is the absolute temperature. The rheology parameters (B^*, n, Q, and V^*; Table 1) are derived from laboratory studies of rock deformation, and f is the scaling parameter. This linearly scales the viscosity relative to the laboratory results to investigate materials that are stronger or weaker owing to moderate changes in composition or water content, or uncertainty in the rheological parameters [*Beaumont et al.*, 2006]. The crust uses the rheological parameters of wet quartzite [*Gleason and Tullis*, 1995], with $f = 5$ to approximate strong, dry quartzo-feldspathic crust [*Beaumont et al.*, 2004, 2006]. The mantle uses the parameters of wet olivine [*Karato and Wu*, 1993]. For the mantle lithosphere, a variation of f between 1 and 5 is compatible with the range of strengths for different water contents [*Hirth and Kohlstedt*, 2003; *Wang*, 2015]. We use $f = 5$ to approximate lithospheric mantle which is dehydrated and melt depleted. The rheology of pyroxenite is not well defined. *Elkins-Tanton* [2005, 2007] suggests that the region around the pyroxenite root may be slightly weaker than the adjacent mantle. In the reference

Table 1. Material Parameters in the Reference Numerical Models

	Crust	Mantle Lithosphere	Pyroxenite Root	Sublithospheric Mantle
Plastic rheology				
c_0 (MPa)	20	20	20	20
ϕ_{eff}	15°	15°	15°	15°
Viscous rheology				
f	5	5	1	1
A (Pa^{-n} s^{-1})	1.10×10^{-28}	3.91×10^{-15}	3.91×10^{-15}	3.91×10^{-15}
B^* (Pa s$^{1/n}$)^a	2.92×10^6	1.92×10^4	1.92×10^4	1.92×10^4
n	4.0	3.0	3.0	3.0
Q (kJ mol^{-1})	223	430	430	430
V^* (cm^3 mol^{-1})	0	10	10	10
Thermal parameters				
k (W m^{-1} K^{-1})	2.25	3.5	3.5	3.5
A_T (μW m^{-3})	1	0	0	0
c_p (J kg^{-1} K^{-1})	750	1250	1250	1250
Density^b				
ρ_0 (kg m^{-3})	2800	3250	3350	3250
T_0 (K)	900	900	900	900
α (K^{-1})	3.0×10^{-5}	3.0×10^{-5}	3.0×10^{-5}	3.0×10^{-5}

$^a B^* = (2^{(1-n)/n} 3^{-(n+1)/2n}) A^{-1/n}$. This converts the pre-exponential viscosity parameter from uniaxial laboratory experiments (A) to the tensor invariant state of stress of the numerical models (B^*).
^{b}Materials have a temperature-dependent density: $\rho(T) = \rho_0[1 - \alpha(T - T_0)]$, where ρ_0 is the reference density at temperature T_0 and α is the volumetric thermal expansion coefficient.

models, we use the wet olivine rheology with $f = 1$ to represent relatively weak pyroxenite lithosphere. In section 4.1.2, we present a model with $f = 5$ to demonstrate how a strong root affects the removal and melting process.

The thermal-mechanical boundary conditions are given in Figure 1. The top boundary of the model has a temperature of 0°C and is stress free, which allows it to be deflected in response to subsurface dynamics. The side boundaries are free slip and have no heat or material transfer. The asthenosphere is initially adiabatic, with a gradient of 0.4°C/km and potential temperature of 1300°C.

3.2. Melt Calculations

We take a simplified approach to determine melting in the models, as our goals are to demonstrate the materials that could melt during lithosphere removal and to assess how different modes of removal may be recognized. For each model, melting is calculated using the pressure-temperature (PT) conditions during model evolution, using the solidus lines shown in Figure 1. We focus on the melting of the mantle, assuming dry materials. In section 4.3, we assess the conditions under which crustal melting may occur, and in section 5.1, we discuss how the results may change if the materials are partially hydrated. Melting is calculated for the mantle lithosphere and asthenospheric mantle using the dry peridotite solidus of *Katz et al.* [2003]. Melting of the pyroxenite root is determined by assuming its solidus is 150°C lower than that of dry peridotite [e.g., *Hirschmann and Stolper*, 1996]. Where melt occurs, the melt volume is calculated assuming 0.3% melt per °C above the solidus

Table 2. List of Numerical Models

Model Name	Lithosphere Thickness (km)	Initial Moho Temperature (°C)	Root Excess Density (kg/m^3)	Root Rheology	Figure Number
Drip-1	75	979	100	WO$^a \times 1$	2a
Drip-2	115	610	100	WO $\times$ 1	2b
Drip-3	75	979	100	WO $\times$ 5	3a
Drip-4	75	979	60	WO $\times$ 1	3b
Drip-5	90	752	100	WO $\times$ 1	8a
Drip-6	90	752	220	WO $\times$ 1	8b
Delamination-1	75	979	20	WO $\times$ 1	4a
Delamination-2	115	610	100	WO $\times$ 1	4b

^{a}WO = wet olivine [*Karato and Wu*, 1993].

[*Elkins-Tanton*, 2005], which is comparable to the melting behavior of peridotite [*Katz et al.*, 2003] and pyroxenite [*Pertermann and Hirschmann*, 2003]. The rheology and density of materials are not changed due to melting, and there is no melt migration in the models. It is assumed that the melt fraction is sufficiently small that there is a negligible effect on the overall dynamics of the system.

4. Numerical Modeling Results

4.1. Rayleigh-Taylor-Type Instability

4.1.1. Models Drip-1 and Drip-2

4.1.1.1. Model Drip-1

This model uses a thin, hot lithosphere (Figure 1a). Figure 2a shows that the dense pyroxenite root is gravitationally unstable and immediately starts to founder. The lengthscale and timescale of foundering depend on the viscosity and density structure [e.g., *Houseman and Molnar*, 1997; *Molnar and Houseman*, 2004]. In this model, the wavelength is ~50 km, and initial foundering occurs as a symmetric pair of drips at each side of the root that detach at ~1.6 Myr. The dense drip induces stresses in the overlying crust (Wang and Currie, submitted); the time of detachment is taken as the time when these stresses decrease, even though there is still a tailing conduit of root material. The first detachment is followed by a pair of drips in the central part of the root at ~2.2 Myr and a final drip at the root center at ~3 Myr. Each drip has a residual tail that continues to descend after the main drip. The drip events remove most of the root material, leaving a ~10 km thick root in the upper plate. Meanwhile, hot asthenosphere upwells to fill the space created by root removal. The surface above the dense root subsides symmetrically, followed by isostatic uplift as the root detaches. After detachment, the surface remains as a slight topographic low, as some root material remains below the crust.

To show where melting may occur, we change the color of pyroxenite lithosphere from dark blue to red and the color of peridotite asthenosphere from white to pink when they cross their dry solidi (Figure 2a). The peridotite mantle lithosphere is also monitored for melting, but it remains below its solidus. In this model, the heads of the drips descend rapidly and remain below their solidus. Starting at ~1.6 Myr, the pyroxenite root that remains within the lithosphere starts to melt as a result of heating associated with lithospheric removal. By 3 Myr, the molten pyroxenite extends across the width of the root. In addition, the narrow pyroxenite tails sink slowly and are conductively heated above their solidus. Figure 2b shows the temporal evolution of the volume of molten pyroxenite (per kilometer perpendicular to the model plane). There is a rapid increase in melt volume at ~2 Myr, owing to heating by the upwelling asthenosphere. Melting continues to increase over time to a maximum of ~50 km^3/km at 3.7 Myr.

The model also predicts significant decompression melting of the upwelling asthenosphere during root removal (Figure 2a). Melting starts at ~2 Myr, after sufficient lithosphere has been removed, and the asthenosphere can upwell to depths less than ~70 km. The onset of asthenospheric melting occurs ~0.4 Myr later than that of lithospheric pyroxenite, but the melting volume increases rapidly, reaching a maximum of ~160 km^3/km at ~3 Myr (Figure 2c). After this, the melt volume decreases, owing to conductive cooling from the overlying lithosphere. The asthenosphere melts are only a few degrees above their solidus and are more sensitive to surface cooling than the pyroxenite melts.

In this model, the first melts are pyroxenites, and their average temperature increases from ~1130°C to ~1260°C between 1.6 and 2.2 Myr, corresponding to the growth and detachment of the first two pairs of drips (Figure 2d). The increase in temperature reflects the fact that initial melting is at ~50 km depth but extends to >100 km depth by 2.2 Myr (Figures 2a and 2e). The average temperature then decreases to ~1180°C at ~3 Myr (Figure 2d). The average depth also decreases over time (Figure 2e), as the majority of melt originates from the residual pyroxenite in the lithosphere (Figure 2a). The peridotite melt temperature is ~1320°C throughout model evolution (Figure 2d). This corresponds to near-adiabatic melting of asthenospheric mantle between depths of ~50 and ~70 km (i.e., between the base of the residual lithosphere and the intersection of the adiabat and solidus) (Figure 2e).

4.1.1.2. Model Drip-2

Model Drip-2 examines RT removal for a thicker and cooler lithosphere, representative of average Phanerozoic lithosphere (Figure 1b). Owing to the cooler lithosphere, only the lower ~40 km of the root participates in the gravitational instability (Figure 2b). Two perturbations grow at the root edges. These rapidly converge, with a final detachment at ~0.5 Myr. A ~12 km wide tail continues to sink for ~50 Myr. The surface
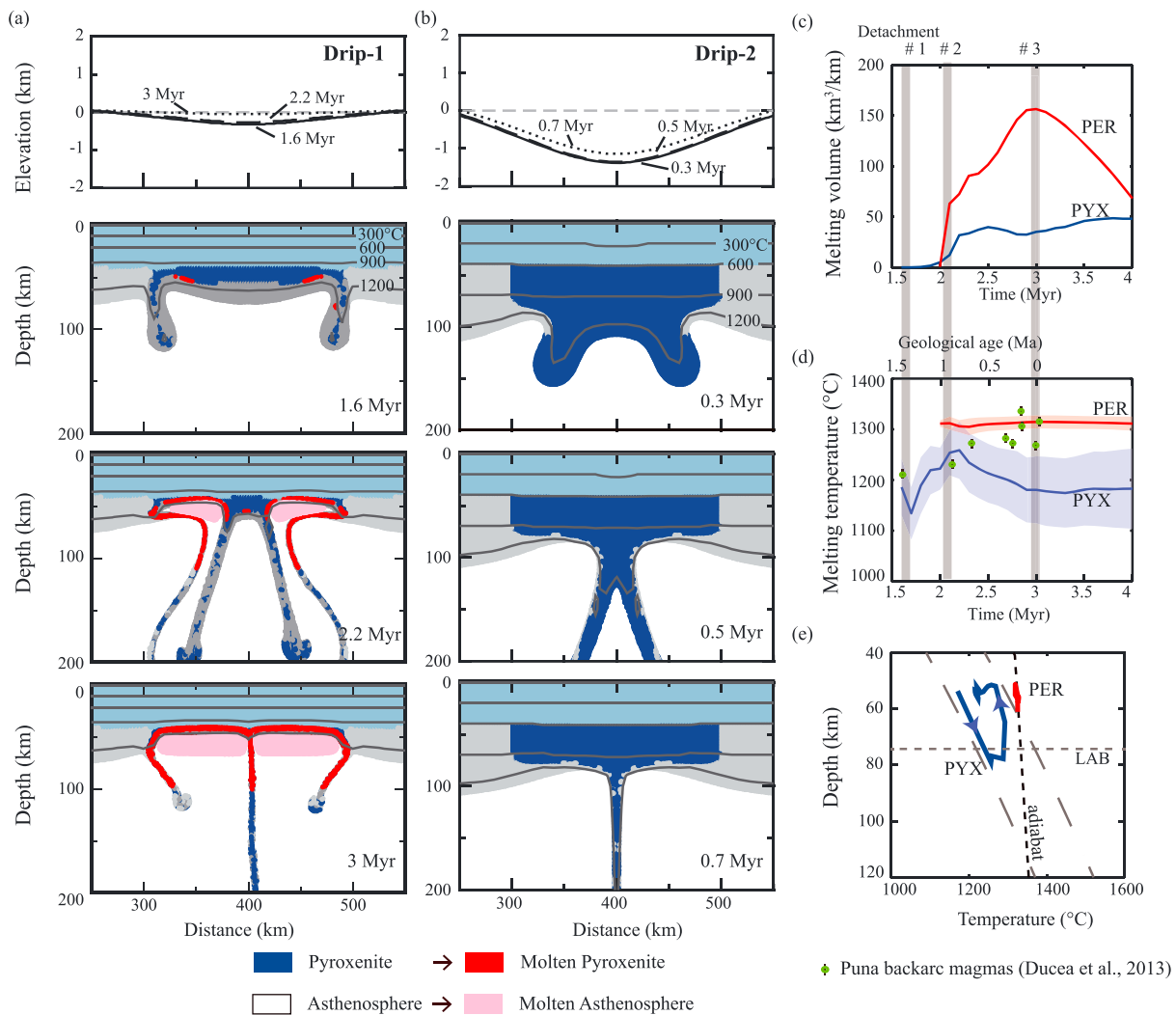
Figure 2. Evolution of (a) Model Drip-1 and (b) Model Drip-2. The top plot is the surface elevation, and the lower plots are the model geometry at the given times. Red and pink show partial melting of lithospheric pyroxenite (PYX) and asthnospheric peridotite (PER), respectively. (c) Predicted melt volume (per kilometers along strike) over time for pyroxenite and peridotite. The grey bars show the time at which drips detach from the upper plate in Drip-1. No melts are predicted for Drip-2. (d) The average (solid lines) and variation (shaded area) of melting temperatures over time for Drip-1. The green circles and error bars are observed melting temperatures of magmas in the Puna plateau; geological ages are along the top axis [*Ducea et al.*, 2013]. (e) Average melting temperature and depth for Drip-1. LAB = lithosphere-asthenosphere boundary.

deflection is similar to Drip-1 but with a larger magnitude of subsidence. In this model, neither lithosphere nor asthenosphere crosses their solidi, and no melting is predicted. The drips sink rapidly and have insufficient time for conductive heating. The thick residual lithosphere is too cool to be heated above its solidus, and its large thickness prevents the asthenosphere from upwelling to a depth where it can undergo decompression melting.

4.1.2. Variations in Other Parameters

In this section, we examine the effects of root viscosity, density, thickness, and width on the magmatism that results from RT-style removal.

4.1.2.1. Root Viscosity

Model Drip-3 tests a 75 km thick lithosphere with a stronger root rheology ($f = 5$), corresponding to the highest viscous strength of olivine [*Hirth and Kohlstedt*, 2003; *Wang*, 2015]. The other parameters are identical to those in Model Drip-1. Figure 3a shows that the high root strength retards the gravitational instability until ~14 Myr. The width of the drips is larger than in Model Drip-1, as expected for an increased viscosity [e.g., *Molnar and Houseman*, 2004]. The drips merge to form a single drip in the center of root at 17.4 Myr, which detaches at 17.8 Myr. In this model, melt is mainly derived from the asthenospheric peridotites that upwell
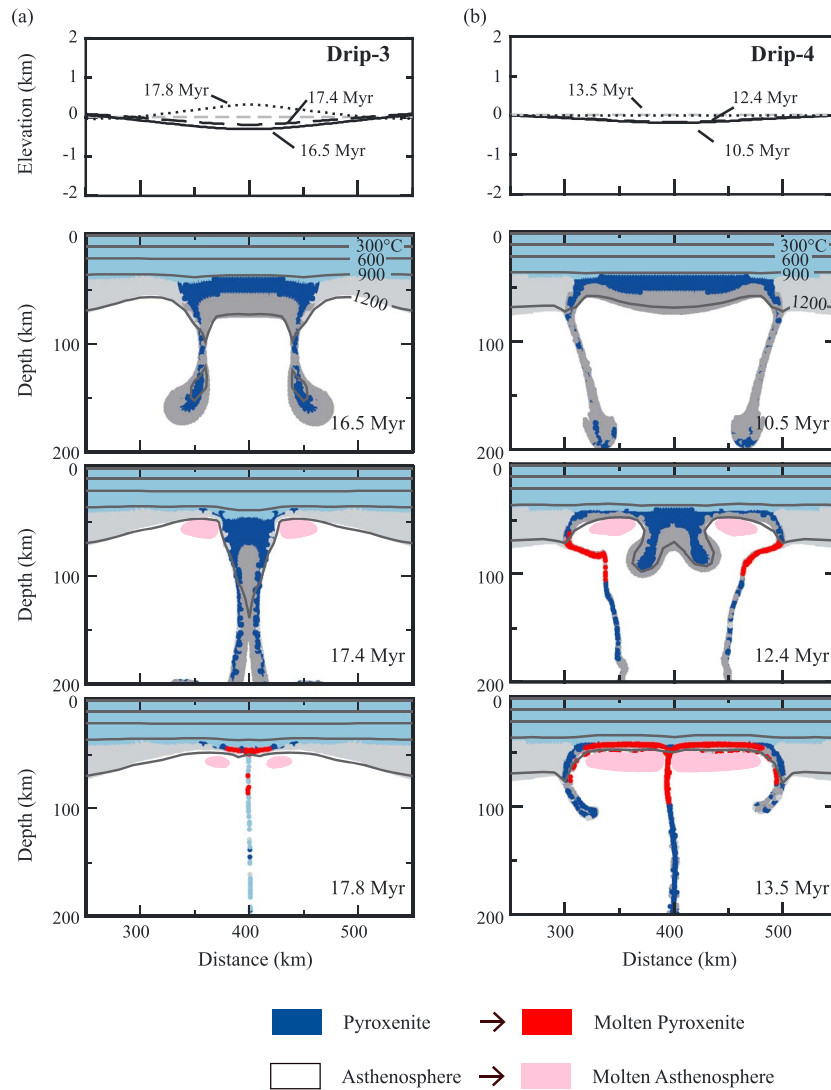
Figure 3. Evolution of (a) Model Drip-3 (with stronger lithosphere rheology) and (b) Model Drip-4 (with lower root density). The top plot is the surface elevation, and the lower plots are the model geometry at the given times.

as the root is removed. After detachment, there is a small amount of melting of the residual lithospheric pyroxenites as they are conductively heated. The drip causes lateral entrainment of the overlying crust, leading to crustal thickening of ~5 km. The surface above the root initially subsides to a maximum depth of 0.35 km and then uplifts to a topographic high (~0.2 km) as a result of crustal thickening.

4.1.2.2. Root Density

The density of the pyroxenite root can be 50 to 250 kg/m^3 more dense than mantle [*Jull and Kelemen*, 2001]. Model Drip-4 tests a relatively low-density root (excess density of 60 kg/m^3), with the other parameters as in Model Drip-1. Figure 3b shows that the low-density root delays the removal until ~10 Myr. The dripping style and wavelength are similar to those in Drip-1, with pairs of drips at the sides and center of the root. Partial melting occurs in the pyroxenite lithosphere first and then in the upwelling asthenosphere. The magma sources and order of melting are similar to those in Drip-1. One difference is that the magma volumes are smaller in Drip-4, owing to surface cooling over the longer time period.

4.1.2.3. Root Thickness

For both lithosphere thicknesses, we have tested variations in root thickness. An increase in root thickness increases the negative buoyancy of the root and affects the removal timescale. For the 75 km lithosphere model, a thicker root that extends through the entire mantle lithosphere is more unstable, resulting in a faster

detachment time and a greater surface deflection than in Model Drip-1. The deep part of this root is above the pyroxenite solidus at the beginning of the model, and therefore, the overall volume of pyroxenite magma is greater. However, the components that melt (both pyroxenite and peridotite) and their relative timing are the same as in Drip-1. For the 115 km thick lithosphere model, a thinner root (15 km thick) does not induce lithosphere removal, as it is located in the shallow, cool part of the lithosphere, where the viscosity is highest. Therefore, no removal or magmatism is predicted.

4.1.2.4. Root Width

The observed width of lithosphere removal varies in different regions. Arc batholith roots are ~100 km wide [e.g., *Saleeby et al.*, 2012]. Removal below orogenic belts affects a 150–600 km wide region [e.g., *Hoke and Garzione*, 2008; *Molnar and Houseman*, 2013]. Intracratonic basins may be associated with a 100–500 km wide density anomaly [*Naimark and Ismail-Zadeh*, 1995]. The above models use a 200 km wide dense root. We have also tested widths of 100–400 km and find that this does not affect the overall removal dynamics. The wavelength of RT instabilities is less than 100 km in our models, and therefore, the root width primarily determines how many drips occur. The width controls the lateral extent of lithosphere removal and therefore the volume of magmatism scales with root width, but the types of melt are not affected.

In summary, variations in the root viscosity, density, thickness, and width can modify the timescale and topographic expression of removal. However, the composition and PT evolution of the predicted melts are not strongly sensitive to these parameters. Instead, the initial thermal structure of the lithosphere has a greater effect on the melts.

4.2. Delamination

The other end-member style of lithosphere removal is delamination. We present delamination models for the two lithosphere thicknesses (Figure 1).

4.2.1. Model Delamination-1

Figure 4a shows the model with a 75 km thick lithosphere. Delamination proceeds slowly, and there is little topographic expression, as the root is only 20 kg/m^3 more dense than mantle. As the lithosphere is removed, asthenosphere upwells and comes into contact with the crust. The deep part of the root may be melted as it is conductively heated during removal. The volume of molten pyroxenite is <10 km^3/km (Figure 4c). This model also predicts a small amount of melting of the upwelling asthenosphere peridotite. The relatively long timescale for delamination (~14 Myr) means that the shallow mantle is cooled from the surface, and therefore, the volume of peridotite melt is suppressed. In this model, the foundering lithosphere melts first, followed by the asthenosphere (Figure 4d), and surface magmatism is expected to migrate from right to left with lithosphere detachment.

4.2.2. Model Delamination-2

For the model with 115 km thick lithosphere, delamination initiates quickly at the right side of the root (Figure 4b). The dense root peels away from the upper plate at a detachment point that migrates leftward. The surface above the root initially subsides and then uplifts to a topographic high. The surface rebound migrates laterally as delamination proceeds. The surface deflection is asymmetric, in contrast to the symmetric deflection associated with RT-style removal. Delamination occurs quickly, and the entire root is removed within 1.1 Myr. The rapid removal means that the pyroxenite root remains below its solidus during detachment. However, widespread decompression melting of the asthenosphere is predicted. The amount of melt increases as the lithosphere detaches, with a maximum of 230 km^3/km at 0.94 Myr (Figure 4c). The melt has an average temperature of ~1310°C (Figure 4d) and originates at depths of 40–60 km (Figure 4e). The volume of peridotite melt in this model is much greater than in the drip models as delamination efficiently removes the entire root region.

We have tested other densities and thicknesses for the pyroxenite root in both delamination models. A high density or large thickness leads to rapid delamination, which is dominated by large-volume asthenosphere melts. Pyroxenite melts are produced if delamination occurs slowly, owing to a low root density or thickness, and melting is enhanced for lithosphere that is initially warm and thin. In all cases, relatively low melt volumes of pyroxenite are predicted.

4.3. Crustal Melting

In this study, we are primarily interested in the types of mantle melts that may be produced by lithosphere removal. However, removal may also induce crustal melting, as the upwelling asthenosphere advects heat to the overlying residual lithosphere [e.g., *Kay et al.*, 2011]. The generation of crustal melts depends on the crustal solidus. This in term depends on the composition and volatile content, which can both be highly
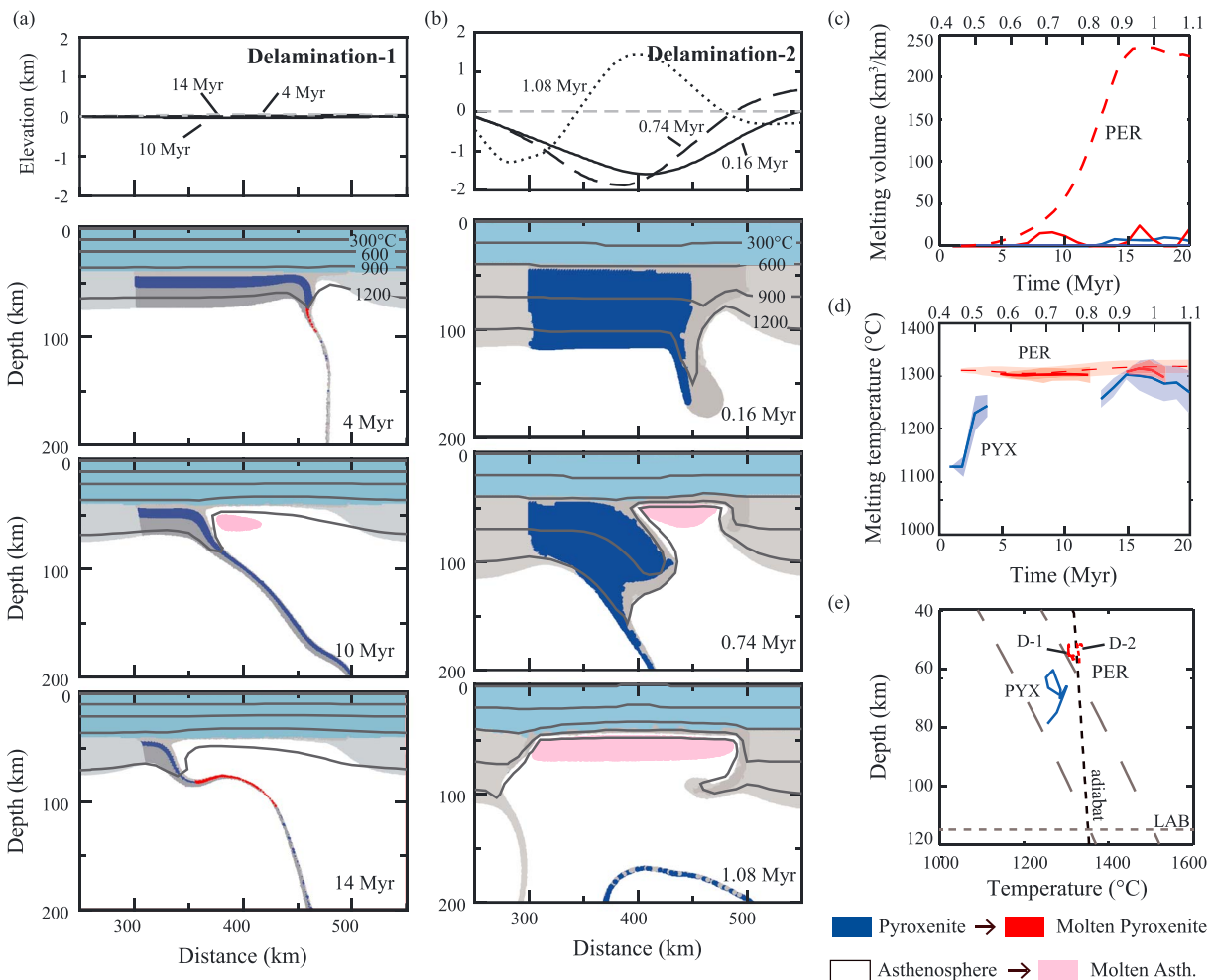
Figure 4. Evolution of (a) Model Delamination-1 and (b) Model Delamination-2. The top plot is the surface elevation, and the lower plots are the model geometry at the given times. (c) Predicted melting volume (per kilometers along strike) over time, (d) average melting temperature over time, and (e) average temperature and depth for melts of pyroxenite (PYX) and peridotite (PER). Solid lines are for Model Delamination-1 (D-1); dashed lines are for Model Delamination-2 (D-2). LAB = lithosphere-asthenosphere boundary.

variable [e.g., *Nair and Chacko*, 2008]. Here we address possible crustal melting using the dry granite solidus [*Elkins-Tanton*, 2005; *Saleeby et al.*, 2012]. A more felsic and/or hydrated crust would have a lower solidus [e.g., *Lindsay et al.*, 2001].

4.3.1. Rayleigh-Taylor-Type Instability

A RT drip involves the part of the dense root that is weak enough to be removed [*Conrad and Molnar*, 1999]. As the root viscosity depends on temperature, the shallow, cold part of the root may be too viscous to be removed, even though it has a high density. The Moho temperature plays an important role in determining the residual lithosphere thickness following a removal event [*Jagoutz and Behn*, 2013]. A hotter Moho results in a weaker mantle lithosphere, and a greater thickness of material can be gravitationally removed, leaving a thinner residual lithosphere. Indeed, the thickness of residual mantle lithosphere in our models is ~10 km when the Moho temperature is 979°C (Drip-1) and ~40 km for a 610°C Moho (Drip-2). As a result of the differing residual thicknesses, the deep crust experiences different magnitudes of heating following removal. Figure 5a shows that the Moho temperature is increased by 100–150°C within 20 Myr for Model Drip-1 but only ~50°C for Model Drip-2.

Figure 5b shows how the temperature-depth structure changes over time at the center of the root (distance = 400 km) and 50 km away from the center (distance = 350 km). For Model Drip-1, the temperature profiles at $x = 350$ km show an earlier heating than the profiles at $x = 400$ km. During root removal, the deep
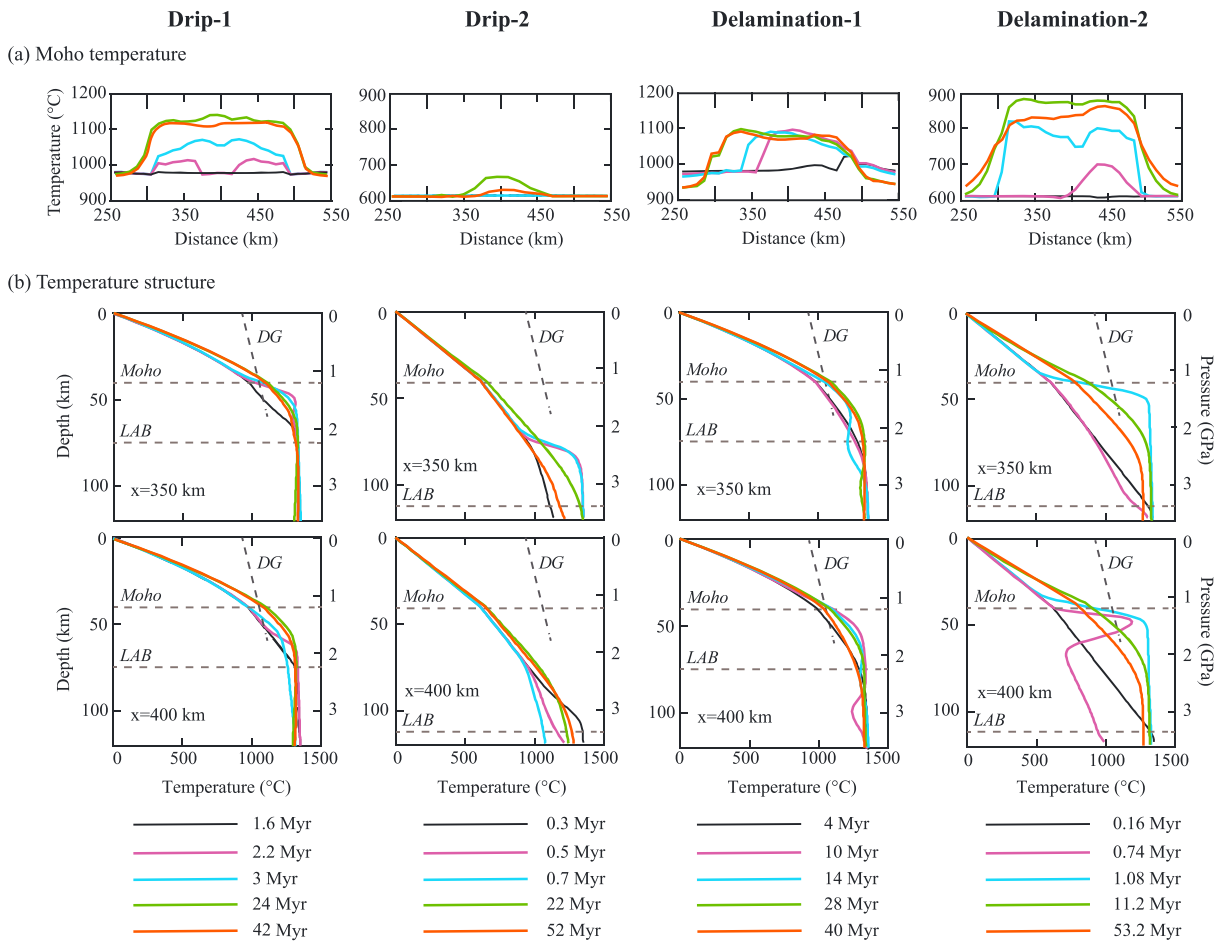
Figure 5. Thermal evolution of Models Drip-1, Drip-2, Delamination-1, and Delamination-2. (a) Moho temperature. (b) Vertical temperature profile at $x = 350$ km (top plot) and $x = 400$ km (bottom plot). The inclined dashed lines show the solidus for dry granite (DG).

crust at $x = 350$ km may become hot enough to melt at ~3 Myr, whereas the crust at $x = 400$ km remains below the solidus. This is consistent with the dynamics of root removal, as removal initially occurs on the edges of the root, and the final removal is at the center (Figure 2). The crust above the root region experiences significant conductive heating to >1100°C following root removal, which places it above the dry granite solidus. This is consistent with earlier studies that show significant lithosphere thinning can cause dry crustal melting at temperatures >1000°C [*Gorczyk and Vogt*, 2013; *Gorczyk et al.*, 2015]. In contrast, if a drip occurs in thicker, cooler lithosphere (Drip-2), only the lowermost root is removed, which leads to only minor heating of the crust, and the crust remains below its solidus throughout removal.

4.3.2. Delamination

Through delamination, the entire dense root can be removed, bringing the hot asthenosphere into direct contact with the deep crust (Figure 4). This leads to rapid crustal heating, which migrates laterally with the detachment point of the dense lithosphere. For a lithosphere that is initially hot and thin (Delamination-1), the temperature at the Moho increases by 100–120°C, and the lower ~5 km of the crust can be heated above the dry granite solidus. In Model Delamination-2, the mantle lithosphere peels away rapidly, causing deep crustal temperatures to increase by ~300°C. The crust is initially cool, and thus, it remains below the dry granite solidus.

5. Discussion

5.1. Numerical Model Predictions of Melting

The main objective of this study is to address the types of mantle melts that may be generated by lithosphere removal via RT-type instability and delamination. For a hot lithosphere, RT-type removal results in significant

lithosphere thinning, which induces melting of both the pyroxenite lithosphere and upwelling peridotite asthenosphere (Model Drip-1). In contrast, a cooler, thicker lithosphere experiences less thinning and neither the lithosphere nor asthenosphere melts (Drip-2). Delamination involves wholesale removal of the mantle lithosphere. Therefore, asthenospheric melts are predicted in all cases, with increased volumes for faster delamination (e.g., more dense root or cooler temperatures). Lithospheric melts may only occur in cases with relatively slow delamination (e.g., due to a low negative buoyancy of the root) and where the lithosphere is initially hot.

In the analysis of melting, it was assumed that all materials are dry. Adding water to either lithosphere or asthenosphere decreases the solidus temperature, enhancing the possibility of melt. The upper mantle may contain 5% H_2O [*Hirschmann and Stolper*, 1996; *Lee et al.*, 2009], which lowers the solidus by ~144°C (Figure 1, right; *Katz et al.*, 2003). In addition, it is possible that the pyroxenite root is partially hydrated. The average water content in the root of the Sierra Nevada batholith is 1% H_2O [*Ducea*, 2002]. The effects of water on the pyroxenite solidus are not well known. For peridotite, 1% H_2O lowers the solidus by 43°C (Figure 1, right; *Katz et al.*, 2003). If the pyroxenite solidus is reduced by a similar amount, the lithosphere will be more susceptible to melting. If both lithosphere and asthenosphere are hydrated in Model Drip-1 (Figure 2a), a greater volume of magma sourced from lithosphere and asthenosphere will be produced, compared to dry models. For Model Drip-2 with a cooler lithosphere (Figure 2b), decompression melting of hydrated asthenosphere is predicted, but the sinking lithosphere still does not cross the solidus line. For Model Delamination-1 (Figure 4a), the addition of water will induce more melt of both lithosphere and asthenosphere. In Model Delamination-2 (Figure 4b), the dense lithosphere sinks rapidly and no melts are predicted, even for hydrated conditions. However, a greater volume of asthenosphere magmas can be produced if the asthenosphere is hydrated.

An additional consideration is the composition of the root material. If the root has a dry peridotite composition, rather than dry pyroxenite, the solidus temperature will be ~150°C higher [*Hirschmann and Stolper*, 1996; *Pertermann and Hirschmann*, 2003]. For all the models shown above, the mantle lithosphere remains below its solidus and no melting is predicted for either RT-type instability or delamination. The volume of asthenosphere melts is not affected.

5.2. Theoretical Predictions of Melting Regimes for Rayleigh-Taylor-Type Instability

A key result from the numerical models is that the predicted melts depend on the initial lithosphere thermal structure (and therefore lithosphere thickness). In this section, a simplified theoretical analysis is used to extend the melt predictions for a RT-type drip to other lithosphere thermal structures and root densities.

5.2.1. Peridotite Melting

First, we consider the conditions under which asthenosphere will melt. This requires that removal causes significant lithospheric thinning, which allows asthenosphere to upwell to a depth where it is above its solidus. Owing to the strongly temperature-dependent lithosphere rheology, only the lower part of a dense lithosphere layer is hot and weak enough to be removed; the upper part is cool and remains stable [*Conrad and Molnar*, 1999] (Figure 6a, right). The thickness of the stable lithosphere determines the minimum depth of asthenospheric upwelling.

To estimate the thickness of stable (or residual) lithosphere, we assume that this layer is resistant to gravitational instability over a long geological time [e.g., *Conrad and Molnar*, 1999; *Jull and Kelemen*, 2001; *Behn et al.*, 2007]. Linear analysis shows that the timescale for RT instability is [*Molnar et al.*, 1998; *Jull and Kelemen*, 2001]

$$t = \left(\frac{B_0}{g\Delta\rho L}\right)^n \left(\frac{n}{C}\right)^n \frac{(Z_0/L)^{(1-n)}}{(n-1)} \tag{2}$$

where B_0 is a rheological coefficient, g is the gravitational acceleration (9.8 m s^{-2}), L is the viscous decay length, n is the rheological exponent, C is a dimensionless geometrical factor, Z_0 is the initial displacement at the base of dense root (assumed to be $Z_0 = 0.01 L$), and $\Delta\rho$ is the density difference between dense root (ρ_{root}) and convecting mantle (ρ_m):

$$\Delta\rho = \rho_{root} - \rho_m + \alpha\rho_m(T - T_m) \tag{3}$$

where α is the coefficient of thermal expansion (3×10^{-5} K^{-1}), T is absolute temperature, and T_m is the adiabatic temperature of the convecting mantle (1573 K + 0.4 K/km × depth).
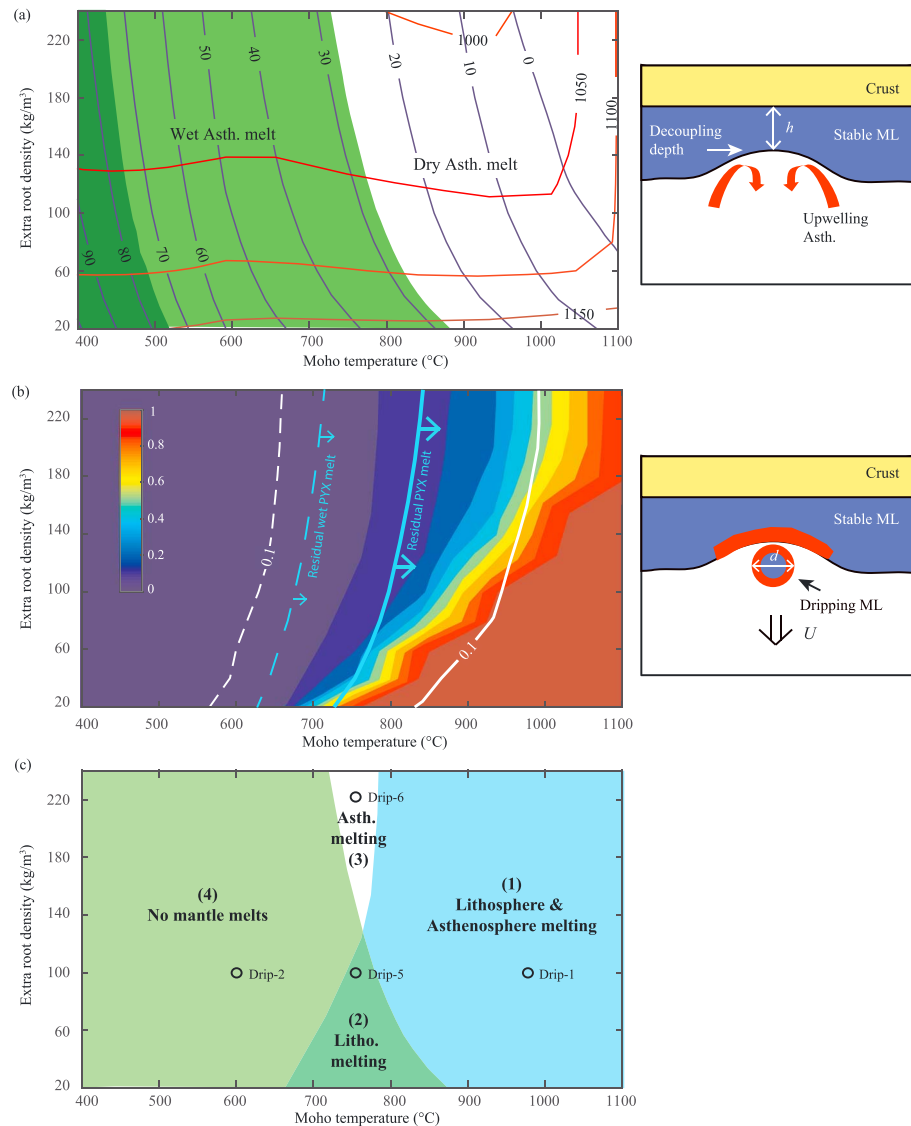
Figure 6. Theoretical predictions for mantle melts generated by RT-type instability for a range of lithosphere thermal structures (denoted by Moho temperature; see Figure 1 for geotherms) and pyroxenite root densities. (a) Conditions for peridotite asthenosphere melts (left) and schematic diagram of calculations (right). Dark green shows where no melts occur; light green shows melting of wet mantle (5% H_2O); white shows melting of wet or dry mantle. Blue contours give the root thickness that is stable over 100 Ma (in kilometers below the Moho). Red contours are temperature at the base of stable lithosphere (given by original geotherm). (b) Conditions for pyroxenite lithosphere melts (left) for residual and foundering material (shown schematically on right). Blue lines are the minimum temperature required for residual root melting for dry (solid line) and wet (1% H_2O, dashed line) lithosphere. Colors show melting fraction of foundering dry pyroxenite lithosphere, approximated as a falling sphere with diameter 10 km. Dashed white line shows the temperature for 10% melting of a sphere with 1% H_2O; solid white line shows the minimum temperature for 10% melting of a 15 km diameter dry sphere. (c) Four melting regimes for dry lithosphere and asthenosphere, assuming 10 km diameter spheres. ML = mantle lithosphere; PYX = pyroxenite; Litho. = lithosphere; Asth. = asthenosphere.

In equation (2), B_0 is the rheological coefficient at base of the stable lithosphere (temperature T_0), where $B(T)$ is

$$B(T) = \frac{1}{2}A^{-1/n}\exp\left(\frac{Q}{nRT}\right) \tag{4}$$

where A is a constant, Q is the activation energy, and R is the universal gas constant (8.3145 J K^{-1}). We use the parameters of wet olivine, where $n = 3$, $A = 3.91 \times 10^{-15}$ Pa^{-n} s^{-1}, and $Q = 430$ KJ mol^{-1} [*Karato and Wu*, 1993]. The geometrical factor is $C = 0.4$ for a nonlinear viscosity with $n = 3$ [*Molnar et al.*, 1998].

For a temperature-dependent viscosity, the rheology coefficient B decreases exponentially with depth over a scaling length L [*Molnar et al.*, 1998]. The viscosity ratio between top and base of stable lithosphere is

$$B_{Moho} = B_0 \exp\left(\frac{h}{L}\right) \tag{5}$$

where B_{Moho} is rheology coefficient at the Moho (temperature T_{Moho}) and h is the stable root thickness.

Equation (2) is used to find the layer thickness that is stable over a timescale of 100 Myr for the range of lithosphere thermal structures shown in Figure 1 (right) and compositional density difference between root and mantle ($\rho_{root} - \rho_m$) of 20 to 240 kg/m^3. Figure 6a shows the predicted stable root thickness for each combination of lithosphere thermal structure (given by the Moho temperature) and excess root density. The main control on the stable thickness is the Moho temperature; a cooler Moho results in a stronger lithosphere that is more resistant to thinning, as also found by *Jagoutz and Behn* [2013]. The root density has a secondary effect on the stable thickness. For a given Moho temperature, the stable thickness decreases with increasing root density, with <20 km variation in thickness for the densities we have tested.

The stable thickness corresponds to the shallowest depth that asthenosphere may upwell following lithosphere removal. A dry, adiabatic asthenosphere must upwell to a depth less than 67 km in order to melt (Figure 1). Figure 6a shows that this occurs for lithosphere with a Moho temperature greater than ~880°C for an excess root density of 20 kg/m^3 and ~730°C for 240 kg/m^3. If the asthenosphere is partially hydrated, upwelling must reach a depth less than 115 km (Figure 1), and thus, the lithosphere must have an initial Moho temperature greater than 440–520°C to enable melting (Figure 6a). For cooler lithospheres, gravitational removal will not produce asthenospheric melts.

5.2.2. Pyroxenite Melting

In the numerical models, lithospheric melts are produced in two ways: (1) conductive heating of the residual root by upwelling asthenosphere and (2) conductive heating of root material as it downwells (e.g., Figure 2). We present simplified calculations to predict whether lithosphere melts may occur for a range of lithosphere thermal structures and root densities.

To calculate residual root melting, we assume that the stable lithosphere (initial temperature T_0) is instantaneously underlain by adiabatic asthenosphere (initial temperature T_m). Over time, the lower lithosphere is conductively heated from below, while the shallow asthenosphere is conductively cooled from above. The time-dependent temperature distribution [$T(t,y)$] near the base of the stable lithosphere is given by [*Turcotte and Schubert*, 2002]

$$\frac{T(t,y) - T_0}{T_m - T_0} = \frac{1}{2} \, erfc\left(\frac{y}{2\sqrt{\kappa t}}\right) \tag{6}$$

where y is distance from the lithosphere-asthenosphere boundary, t is time, and κ is the thermal diffusivity (10^{-6} m^2/s).

For each combination of lithosphere thermal structure and root density, the temperature evolution of the lowermost stable lithosphere is calculated and the temperatures are compared to the dry pyroxenite solidus (Figure 1, right). Figure 6b shows the conditions under which a ≥5 km thick pyroxenite lithosphere layer can melt within 10 Ma. Melting of dry pyroxenite is predicted for Moho temperatures greater than ~720–840°C for excess root densities of 20–240 kg/m^3. Melting is more restricted with a denser root because this causes a greater thinning of the lithosphere (Figure 6a), and therefore, the base of the stable lithosphere has an initially lower temperature. If instead the pyroxenite is hydrated, the residual lithosphere may melt for Moho temperatures greater than 620–700°C, owing to the lower solidus temperature (Figure 6b).

The second lithospheric melt component results from conductive heating of the foundering root. Following *Elkins-Tanton* [2005], we approximate the foundering root as a sphere that falls through an adiabatic asthenosphere. The Stokes flow equation [*Turcotte and Schubert*, 2002] is used to calculate the sinking velocity of the sphere with a density contrast of $\Delta\rho$ relative to the surrounding mantle:

$$U = 2\frac{(d/2)^2 g\Delta\rho}{9\mu_{asth}} \tag{7}$$

where d is the diameter of sphere and μ_{asth} is the viscosity of asthenosphere (taken as 10^{19} Pa s). As the sphere falls, it is heated by the surrounding asthenosphere, and the temperature evolution [$T(t,y)$] is given by [*Turcotte and Schubert*, 2002]

$$\frac{T(t,y) - T_0}{T_m - T_0} = erfc\left(\frac{y}{2\sqrt{\kappa t}}\right) \tag{8}$$

where T_0 is the initial temperature of sphere, T_m is the adiabatic mantle temperature, y is the distance from the edge of sphere toward its center, and κ is the thermal diffusivity (10^{-6} m^2/s).

For each combination of lithosphere thermal structure and root density, we track the thermal evolution of a sphere that starts at the base of the stable lithosphere, with a temperature given by the geotherm at that depth (Figure 6a). Temperatures are calculated as the sphere falls through the adiabatic mantle at velocity U to a depth of 115 km (the intersection between the dry pyroxenite solidus and mantle adiabat; Figure 1). The temperature of sphere is compared to pyroxenite solidus to determine if melting will occur.

Figure 6b shows the predicted melting fraction for dry pyroxenite spheres with a diameter of 10 km. Melting of 10% or more is predicted for lithospheres that have a Moho temperature greater than 670–780°C. The required temperature increases with increasing sphere density as a denser sphere sinks more quickly and thus has less time to heat. For cooler lithospheres, the foundering material has a low initial temperature and is not heated above its solidus during descent. Figure 6b also shows that larger spheres (diameter 15 km) require a higher initial temperature to undergo melting, owing to their more rapid descent rate. The dashed line on Figure 6b shows the minimum temperature-density conditions that are needed if the pyroxenite contains 1% H$_2$O. Melting is predicted for a wider range of lithosphere temperatures, as the presence of water reduces the solidus temperature.

These calculations assume that the lithosphere has a pyroxenite composition. If the lithosphere has a dry peridotite composition, the minimum Moho temperature for melting is larger than 1100°C for both the residual lithosphere and foundering spheres (diameter of 10 km). For a partially hydrated lithosphere (1% H$_2$O), the conditions for melting are comparable to those of dry pyroxenite. This suggests that a dry peridotite lithosphere is unlikely to melt during removal; lithospheric melts are only expected if the lithosphere is hydrated or has a pyroxenite composition.

We note that there are several limitations to the theoretical calculations presented here. For example, the asthenosphere and residual lithosphere melts are calculated assuming that the lithosphere (with a thermal structure given by the conductive geotherms in Figure 1) is instantaneously thinned to its stable thickness and replaced by adiabatic asthenosphere; we do not consider how the thermal structure is modified during the removal process. The stable thickness in Figure 6a is based on the conductive geotherm and does not include later heating which may lead to further thinning as this material is thermally weakened. This also assumes a wet olivine rheology; a stronger rheology results in less lithospheric thinning. Melting of foundering lithosphere is based on a sphere that is fully surrounded by adiabatic mantle, but in reality, the lithosphere detaches as an elongated drip. Nonetheless, the simplified calculations are useful for demonstrating the range of conditions under which melting may be generated, and as we show below, they are broadly consistent with the numerical model results.

5.3. Types of Mantle Melts

On the basis of the calculations in section 5.2, there are four types of mantle melting that may be associated with RT-style removal of mantle lithosphere (Figure 7). The lithosphere temperature and root density conditions for each type are shown in Figure 6c, which combines the results of the analysis of peridotite asthenosphere melts (Figure 6a) and pyroxenite lithosphere melts (Figure 6b), assuming dry materials and 10 km wide drips. If the materials are partially hydrated, the boundaries between the melting types will occur for cooler lithosphere than discussed below.

5.3.1. RT Type 1: Lithosphere and Asthenosphere Melts

This type of magmatism occurs if the lithosphere is relatively warm (Moho >800°C for most root densities; Figure 6c). It is consistent with that shown in Model Drip-1 (Figure 2a). Gravitational instability results in removal of a significant fraction of the lithosphere, and the asthenosphere can upwell to a shallow enough depth to undergo decompression melting. The lithospheric pyroxenite is relatively warm and can be readily
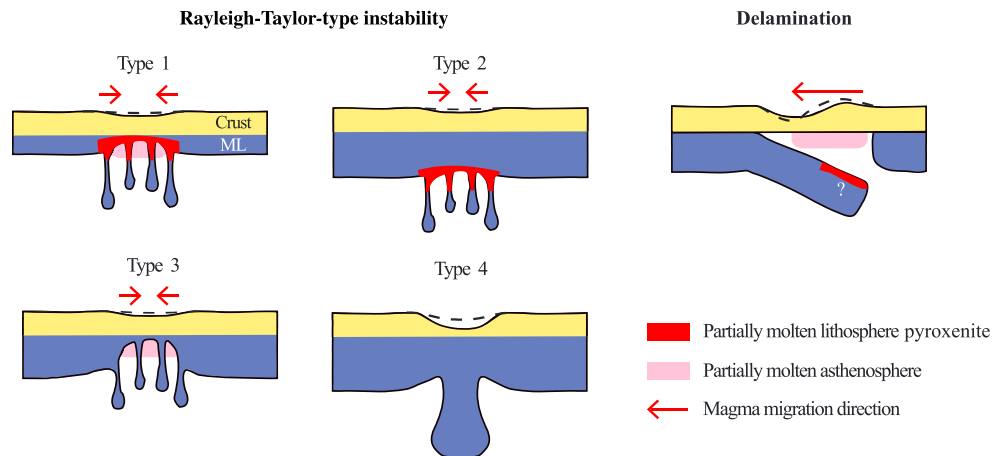
Figure 7. Summary of the four types of mantle-derived magmatism for lithosphere removal through RT-type instability. Delamination is primarily accompanied by asthenospheric melting that migrates laterally; small volumes of lithosphere melts may be generated if delamination occurs slowly or affects warm lithosphere.

heated above its solidus by conductive heating from the asthenosphere. Removal may also trigger melting of the deep crust if the asthenosphere is in close proximity to the base of the crust.

If the foundering pyroxenite root has a weak rheology, this material will melt first, followed by asthenospheric melting (e.g., Drip-1, Figure 2a). Removal is accompanied by subsidence of the surface above the drip and then uplift after drip removal. If the root is stronger, the size of the drips and the timescale for removal increase (e.g., Drip-3, Figure 3a). This delays the onset of root melting, and therefore, the asthenosphere may melt first. The root may cause thickening of the overlying crust, leading to surface uplift during drip removal [e.g., *Neil and Houseman*, 1999; *Pysklywec and Beaumont*, 2004; *Wang and Currie, submitted*]. In both cases, melting should initiate at the edges of the root region and migrate toward the center (Figure 7). The surface topography will also be symmetric above the foundering lithosphere.

5.3.2. RT Type 2: Only Lithosphere Melts

This type is predicted at moderate lithosphere temperatures (Moho 670–860°C) and where the excess density of the pyroxenite root is low ($<120 \, kg/m^3$) (Figure 6c). With the low density, the foundering lithosphere descends slowly and there is enough time for the drip to be conductively heated above its solidus. However, the low density results in a thicker stable lithosphere, which prevents decompression melting of the asthenosphere. This also limits the amount of heating of the crust, and crustal melts are unlikely. We confirm this type of melt using a numerical model (Model Drip-5) which has a 90 km lithosphere (Moho temperature 752°C) and a pyroxenite root with an excess density of $100 \, kg/m^3$. As shown in Figure 8a, the root destabilizes through a series of small drips and the tails of the drips melt during their descent. However, the residual lithosphere thickness is ~70 km (in agreement with that predicted in Figure 6a), and the asthenosphere does not undergo dry decompression melting.

5.3.3. RT Type 3: Only Asthenosphere Melts

This is predicted for a relatively warm lithosphere (Moho 720–790°C) and a high root density ($>120 \, kg/m^3$ more dense than mantle) (Figure 6c). In this case, the lithosphere can be gravitationally thinned enough to induce decompression melting of asthenosphere. However, the foundering lithosphere descends too quickly and is not heated above its solidus. Both the distribution of asthenospheric magmas and surface subsidence/uplift are symmetric above the foundering root. Depending on the magnitude of lithosphere thinning and the initial temperature and composition of the crust, the crust may melt. Model Drip-6 confirms this type of melt using an excess root density of $220 \, kg/m^3$ and the thermal structure used in Drip-5. Figure 8b shows that the dense lithosphere founders too rapidly to melt. However, the lithosphere is thinned to less than 70 km, which allows the asthenosphere to undergo decompression melting.

5.3.4. RT Type 4: No Mantle-Derived Melts

This type is associated with regions that have an initially thick and cool lithosphere (e.g., Moho <720°C for most root densities; Figure 7c). The numerical model in Figure 2b (Drip-2) is an example of this type. The low temperature increases the root strength, causing it to founder in large drips, which descend too rapidly to be heated
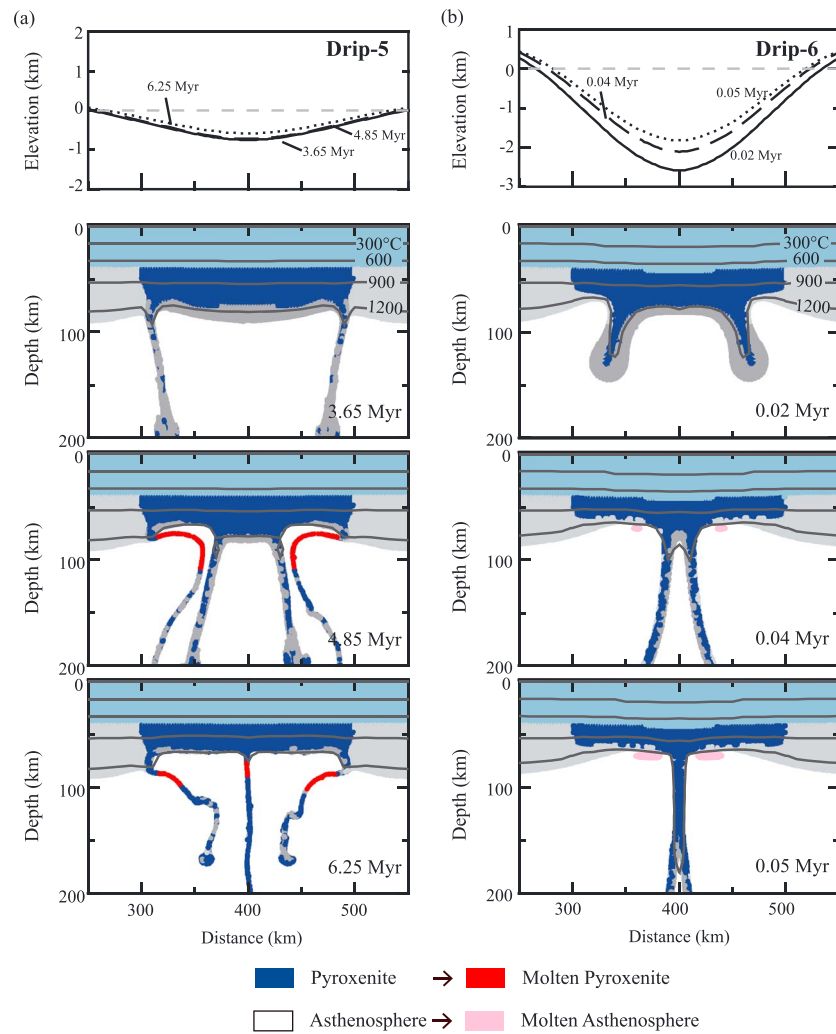
Figure 8. Evolution of (a) Model Drip-5 (excess root density of 100 kg/m^3) and (b) Model Drip-6 (excess root density of 220 kg/m^3). Both models have a 90 km thick lithosphere, with a Moho temperature of 752°C. The pyroxenite root thickness is 35 km (intersection of dry pyroxenite solidus and lithosphere geotherm, Figure 1). The top plot is the surface elevation, and the lower plots are the model geometry at the given times.

above their solidus. In addition, the low temperature limits the amount of removal, and the thick residual lithosphere prevents the upwelling asthenosphere from melting. This also suppresses crustal heating, and crustal melts are not expected. Owing to the cool temperatures, the root and crust are strongly coupled, creating significant subsidence that is symmetric about the drip, followed by partial uplift after drip detachment.

5.3.5. Melts Induced by Delamination

The other end-member style of removal is delamination, in which the entire thickness of mantle lithosphere is removed as a coherent slab that detaches along a shallow weak layer (Figure 7). Our numerical models show that for most lithosphere densities and rheologies, delamination is a rapid process, which allows adiabatic mantle to upwell to shallow depths. Therefore, delamination will typically be accompanied by widespread decompression melting of the asthenosphere. If the lithosphere has a relatively low density or the decoupling layer is stronger, delamination may occur more slowly, which could allow some lithosphere melting to occur, especially for an initially warm lithosphere (e.g., Figure 4a). Delamination also leads to rapid heating of the deep crust, which may produce melting. This type of melting can be differentiated from RT Types 1 and 3 by both the volume of asthenospheric melt and the spatial distribution of melting. Delaminating lithosphere is removed asymmetrically, and magmatism should migrate laterally as the lithosphere detaches. This style of removal may also be recognized by a migrating wave of surface subsidence followed by uplift.

5.4. Geological Implications

Our numerical models demonstrate that removal via RT-type instability and delamination can be differentiated by the spatial distribution of magmatism. In a RT-type instability, magmatism initiates at the edges of the instability and migrates inward (Figures 2 and 3). We expect that in 3D, this would correspond to ring-shaped magmatism that converges radially, but full 3D models are needed to study this in detail. This pattern has been recognized in magmas that have erupted at the edge of the Colorado plateau in the last ~25 Ma, suggesting a link with convective dripping of the lower lithosphere [e.g., *Roy et al.*, 2009; *van Wijk et al.*, 2010]. In contrast, delamination should exhibit an asymmetric surface expression (Figure 4). This is consistent with observations from the North Island of New Zealand, where a lateral migration of surface subsidence/uplift and high-K magmatism have been proposed to be related to lithosphere delamination [*Kear*, 2004; *Stern et al.*, 2013]. High-K magmatism is typically interpreted to indicate crustal melting induced by rapid heating following lithosphere removal [e.g., *Farmer et al.*, 2002]; other studies argue that low-degree melts from the upper mantle can produce this signal [e.g., *Putirka and Busby*, 2007].

The numerical models and theoretical analysis show that both the style of removal and the preexisting thermal structure of the lithosphere strongly control the resulting magmatism. This may explain the diversity of magmatism observations for areas with lithosphere removal, from the absence of magmatism in cratonic regions [e.g., *Elkins-Tanton*, 2005] to widespread magmatism in active orogens [e.g., *Kay et al.*, 1994].

Here we compare our RT-type model results with observations from the southern Puna plateau in South America. This region has a long history of magmatism with diverse compositions, including those that are inconsistent with subduction-related processes [e.g., *Kay and Kay*, 1993; *Kay et al.*, 1994]. *Ducea et al.* [2013] and *Murray et al.* [2015] use the Zn/Fe ratio to understand the origin of the Neogene magmas in this region. They find that the earliest magmas (1.5–1 Ma) are mainly sourced from lithospheric pyroxenites, and later magmas show a progressive increase in the asthenospheric peridotite component. The source temperature increases from 1200°C to 1300°C over a ~1.5 Myr time period (Figure 2d). *Ducea et al.* [2013] suggest that the origin of magmatism and the temporal shift in its composition and temperature are caused by small-scale RT drips.

The observations and interpretation by *Ducea et al.* [2013] are consistent with our RT Type 1 magmas, especially if the dense lithospheric pyroxenite has a relatively weak rheology. This requires that the lithosphere is initially warm. The southern Puna plateau has a thick crust, but the underlying mantle lithosphere is thin (<30 km) [*Babeyko et al.*, 2002; *Schurr et al.*, 2006; *Bianchi et al.*, 2012]. Further, the midcrust is inferred to be 700–800°C at 20–25 km depth [*Babeyko et al.*, 2002, and reference therein], which indicates even higher temperatures at the Moho. The hot, thin lithosphere appears to be a long-lived feature that predates the foundering event [e.g., *Babeyko et al.*, 2002].

As shown in this study, as a warm lithosphere undergoes convective destabilization, lithospheric melting can result from conductive heating of both the residual root and the foundering pieces of root (Figure 2). Lithosphere removal induces upwelling of the asthenosphere, which may undergo decompression melting. At this point, the main magma source changes from lithosphere to asthenosphere, and overall, the average temperature of the melts increases over time. This sequence of events requires that the lithospheric root destabilizes in a series of small drips. We suggest that the Puna lithosphere is hot and partially hydrated due to its position above the subducting Nazca plate. As a result, the lithosphere has a weak rheology, which favors smaller drip sizes.

The southern Sierra Nevada (California) is another place where lithosphere removal has been proposed [e.g., *Ducea and Saleeby*, 1996; *Farmer et al.*, 2002]. Pliocene magmas at the eastern side of the southern Sierra Nevada appear to be derived from metasomatized asthenospheric peridotites at 40–100 km depth [*Farmer et al.*, 2002; *Elkins-Tanton and Grove*, 2003]. A xenolith study shows that the lithosphere was >100 km thick before the Pliocene and that the lithosphere at 40–75 km depth was rich in garnet pyroxenites (~200 kg/m^3 denser than asthenosphere) [*Ducea and Saleeby*, 1998]. Pliocene magmatism was accompanied by significant vertical deflection at surface, with Pliocene uplift at the eastern side and Pliocene-Quaternary subsidence at the western side [*Saleeby et al.*, 2012, and references therein].

Our models show that lithosphere delamination is a possible explanation for these observations. If this is right, the mantle lithosphere beneath the eastern side of the Sierra Nevada probably detached in the Pliocene, driven by the presence of the dense garnet pyroxenite root. The root itself may be a remnant of earlier arc magmatism associated with Farallon Plate subduction [e.g., *Ducea*, 2001]. Detachment likely occurred at the base of the

crust, and this allowed the asthenosphere to upwell to shallow depths where it melted through decompression. The temporal variations in surface uplift and subsidence suggest that lithosphere detachment has migrated westward across the Sierra Nevada. Our model indicates that magmatism should migrate with the delamination hinge (Figure 4). The spatial variation of Cenozoic volcanism in the southern Sierra Nevada is not well known [*Farmer et al.*, 2002]. However, *Saleeby et al.* [2012, 2013] suggest that the 0–4 Ma volcanism mainly occurs in the area with Pliocene surface uplift, while the region that has the most recent rock uplift also exhibits increasing surface heat flow. Seismic studies show an eastward dipping high-velocity anomaly beneath this region [e.g., *Zandt and Carrigan*, 1993; *Jones et al.*, 1994]. The high-velocity anomaly is interpreted to be the mantle lithosphere [e.g., *Saleeby et al.*, 2012], and its geometry is consistent with lithosphere delamination. Below the Tulare Basin (western Sierra Nevada), the mantle lithosphere appears to be coupled to the crust; under the eastern Sierra Nevada, the mantle lithosphere is detached from the crust and is found at ~200 km depth [*Zandt and Carrigan*, 1993; *Jones et al.*, 1994]. Above the eastern region, the Pliocene magmas appear to represent asthenosphere melts with the source depth decreasing from ~100 km to 40–75 km over time; in the Quaternary, the magmas have more a silicic composition [*Moore and Dodge*, 1980; *Saleeby et al.*, 2012]. The variation in melting source and depth is consistent with the prediction of our delamination models (Figure 4), in which melt is first extracted from upwelling asthenosphere and later extends into the lower crust.

6. Conclusions

Magmatism in the interior regions of continental plates may be associated with gravitational lithosphere removal [e.g., *Kay and Kay*, 1993]. Such magmatism carries information about ancient and ongoing lithospheric removal events. In this study, we have used both numerical models and a simplified theoretical analysis to investigate the possible magma sources and the pressure-temperature evolution of magmatism associated with lithosphere removal via RT-type instability and delamination.

The lithosphere thermal structure strongly affects the magmatic expression of a RT-type instability. Four types of magmatism are predicted for dry mantle:

1. Destabilization of a hot, thin lithosphere (e.g., back arc or other tectonically active Phanerozoic area) can induce melting of lithospheric pyroxenites through conductive heating and melting of upwelling asthenospheric peridotites through decompression. Small-scale drips of weak mantle lithosphere are especially prone to melting.
2. For moderately warm lithosphere (e.g., stable Phanerozoic lithosphere) in which the lithosphere root has a low compositional density ($<$120 kg/m^3 denser than asthenosphere), removal only involves a thin layer of the lowermost lithosphere. No decompression melting of the asthenosphere is predicted, but the lithosphere pyroxenites may melt.
3. If the root has a high compositional density ($>$120 kg/m^3 denser than asthenosphere) in a moderately warm lithosphere, the lithosphere founders rapidly and does not melt. However, the lithosphere is significantly thinned, enabling decompression melting of the asthenosphere.
4. If the lithosphere is cold and thick (e.g., craton lithosphere), gravitational removal is limited to the lowermost lithosphere and no magmatism is generated.

These results are dependent on the water content of the lithosphere and asthenosphere. With hydration, the solidus temperature of each composition is reduced, and therefore, melting occurs for a greater range of thermal conditions and the melt volume increases. If lithosphere is composed of dry peridotite, rather than pyroxenite, its solidus temperature will be higher and lithospheric mantle melts are unlikely. Crustal melting can occur if the RT instability results in significant lithospheric thinning; this is confined to regions with lithosphere that is warm and rheologically weak.

In delamination, the entire mantle lithosphere detaches by peeling along the Moho [*Bird*, 1979]. This causes widespread decompression melting of the asthenosphere. The deep crust is rapidly heated, which may result in melting, especially for lithosphere that is initially warm. In most cases, lithosphere detachment occurs rapidly and the foundering lithosphere remains below its solidus. A small volume of lithospheric pyroxenite melt may be generated if the detaching lithosphere has a low density or a high temperature. In the magmatic record, delamination may be recognized by a lateral migration in magmatism, where melting follows the detachment hinge. In contrast, magmatism induced by RT-type instability is symmetric above the drip and may migrate radially toward the center as the drip detaches.

References

Babeyko, A. Y., S. V. Sobolev, R. B. Trumbull, O. Oncken, and L. L. Lavier (2002), Numerical models of crustal scale convection and partial melting beneath the Altiplano–Puna plateau, *Earth Planet. Sci. Lett.*, *199*(3), 373–388.

Beaumont, C., R. A. Jamieson, M. H. Nguyen, and S. Medvedev (2004), Crustal channel flows: 1. Numerical models with applications to the tectonics of the Himalayan-Tibetan orogeny, *J. Geophys. Res.*, *109*, B06406, doi:10.1029/2003JB002809.

Beaumont, C., M. H. Nguyen, R. A. Jamieson, and S. Ellis (2006), Crustal flow modes in large hot orogens, *Geol. Soc. London Spec. Publ.*, *268*, 91–145, doi:10.1144/GSL.SP.2006.268.01.05.

Behn, M. D., G. Hirth, and P. B. Kelemen (2007), Trench-parallel anisotropy produced by foundering of arc lower crust, *Science*, *317*(5834), 108–111.

Bianchi, M., B. Heit, A. Jakovlev, X. Yuan, S. M. Kay, E. Sandvol, R. N. Alonso, B. Coira, and R. Kind (2012), Teleseismic tomography of the southern Puna plateau in Argentina and adjacent regions, *Tectonophysics*, *586*, 65–83.

Bird, P. (1979), Continental delamination and the Colorado Plateau, *J. Geophys. Res.*, *84*(B13), 7561–7571, doi:10.1029/JB084iB13p07561.

Burov, E. B., and A. B. Watts (2006), The long-term strength of continental lithosphere: "Jelly sandwich" or "crème brûlée"?, *GSA Today*, *16*(1), 4.

Chung, S. L., D. Liu, J. Ji, M. F. Chu, H. Y. Lee, D. J. Wen, C.-H. Lo, T.-Y. Lee, Q. Qian, and Q. Zhang (2003), Adakites from continental collision zones: Melting of thickened lower crust beneath southern Tibet, *Geology*, *31*(11), 1021–1024.

Conrad, C. P., and P. Molnar (1999), Convective instability of a boundary layer with temperature- and strain-rate-dependent viscosity in terms of 'available buoyancy', *Geophys. J. Int.*, *139*(1), 51–68.

Currie, C. A., and R. D. Hyndman (2006), The thermal structure of subduction zone back arcs, *J. Geophys. Res.*, *111*, B08404, doi:10.1029/2005JB004024.

Darold, A., and E. Humphreys (2013), Upper mantle seismic structure beneath the Pacific Northwest: A plume-triggered delamination origin for the Columbia River flood basalt eruptions, *Earth Planet. Sci. Lett.*, *365*, 232–242.

DeCelles, P. G., M. N. Ducea, P. Kapp, and G. Zandt (2009), Cyclicity in Cordilleran orogenic systems, *Nat. Geosci.*, *2*(4), 251–257.

DeCelles, P. G., B. Carrapa, B. K. Horton, J. McNabb, G. E. Gehrels, and J. Boyd (2015), The Miocene Arizaro Basin, central Andean hinterland: Response to partial lithosphere removal?, *Geol. Soc. Am. Mem.*, *212*, 359–386.

Ducea, M. N. (2001), The California arc: Thick granitic batholiths, eclogitic residues, lithospheric-scale thrusting, and magmatic flare-ups, *GSA Today*, *11*(11), 4–10.

Ducea, M. N. (2002), Constraints on the bulk composition and root foundering rates of continental arcs: A California arc perspective, *J. Geophys. Res.*, *107*(B11), 2304, doi:10.1029/2001JB000643.

Ducea, M. N. (2011), Fingerprinting orogenic delamination, *Geology*, *39*(2), 191–192.

Ducea, M. N., and J. B. Saleeby (1996), Buoyancy sources for a large, unrooted mountain range, the Sierra Nevada, California: Evidence from xenolith thermobarometry, *J. Geophys. Res.*, *101*(B4), 8229–8244, doi:10.1029/95JB03452.

Ducea, M. N., and J. Saleeby (1998), A case for delamination of the deep batholithic crust beneath the Sierra Nevada, California, *Int. Geol. Rev.*, *40*(1), 78–93.

Ducea, M. N., A. C. Seclaman, K. E. Murray, D. Jianu, and L. M. Schoenbohm (2013), Mantle-drip magmatism beneath the Altiplano-Puna plateau, central Andes, *Geology*, doi:10.1130/G34509.1.

Elkins-Tanton, L. T. (2005), Continental magmatism caused by lithospheric delamination, *Geol. Soc. Spec. Pap.*, *388*, 449–461.

Elkins-Tanton, L. T. (2007), Continental magmatism, volatile recycling, and a heterogeneous mantle caused by lithospheric gravitational instabilities, *J. Geophys. Res.*, *112*, B03405, doi:10.1029/2005JB004072.

Elkins-Tanton, L. T., and T. L. Grove (2003), Evidence for deep melting of hydrous metasomatized mantle: Pliocene high-potassium magmas from the Sierra Nevadas, *J. Geophys. Res.*, *108*(B7), 2350, doi:10.1029/2002JB002168.

Farmer, G. L., A. F. Glazner, and C. R. Manley (2002), Did lithospheric delamination trigger late Cenozoic potassic volcanism in the southern Sierra Nevada, California?, *Geol. Soc. Am. Bull.*, *114*(6), 754–768.

Fullsack, P. (1995), Arbitrary Lagrangian–Eulerian formulation for creeping flows and its application in tectonic models, *Geophys. J. Int.*, *120*(1), 1–23.

Gao, S., et al. (2008), Recycling deep cratonic lithosphere and generation of intraplate magmatism in the North China Craton, *Earth Planet. Sci. Lett.*, *270*(1), 41–53.

Gleason, G. C., and J. Tullis (1995), A flow law for dislocation creep of quartz aggregates determined with the molten salt cell, *Tectonophysics*, *247*(1), 1–23, doi:10.1016/0040-1951(95)00011-B.

Göğüş, O. H., and R. N. Pysklywec (2008), Near-surface diagnostics of dripping or delaminating lithosphere, *J. Geophys. Res.*, *113*, B11404, doi:10.1029/2007JB005123.

Gorczyk, W., and K. Vogt (2013), Tectonics and melting in intra-continental settings, *Gondwana Res.*, *27*(1), 196–208.

Gorczyk, W., H. Smithies, F. Korhonen, H. Howard, and R. Q. De Gromard (2015), Ultra-hot Mesoproterozoic evolution of intracontinental central Australia, *Geosci. Front.*, *6*(1), 23–37.

Hales, T. C., D. L. Abt, E. D. Humphreys, and J. J. Roering (2005), A lithospheric instability origin for Columbia River flood basalts and Wallowa Mountains uplift in northeast Oregon, *Nature*, *438*(7069), 842–845.

Heit, B., M. Bianchi, X. Yuan, S. M. Kay, E. Sandvol, P. Kumar, R. Kind, R. N. Alonso, L. D. Brown, and D. Comte (2014), Structure of the crust and the lithosphere beneath the southern Puna plateau from teleseismic receiver functions, *Earth Planet. Sci. Lett.*, *385*, 1–11.

Hirschmann, M. M., and E. M. Stolper (1996), A possible role for garnet pyroxenite in the origin of the "garnet signature" in MORB, *Contrib. Mineral. Petrol.*, *124*(2), 185–208.

Hirth, G., and D. Kohlstedt (2003), Rheology of the upper mantle and the mantle wedge: A view from the experimentalists, in *Inside the Subduction Factory*, *Geophys. Monogr. Ser.*, vol. 138, edited by J. Eiler, pp. 83–105, AGU, Washington, D. C.

Hoke, G. D., and C. N. Garzione (2008), Paleosurfaces, paleoelevation, and the mechanisms for the late Miocene topographic development of the Altiplano plateau, *Earth Planet. Sci. Lett.*, *271*, 192–201.

Horodyskyj, U. N., C. T. A. Lee, and M. N. Ducea (2007), Similarities between Archean high MgO eclogites and Phanerozoic arc-eclogite cumulates and the role of arcs in Archean continent formation, *Earth Planet. Sci. Lett.*, *256*(3), 510–520.

Houseman, G. A., and P. Molnar (1997), Gravitational (Rayleigh-Taylor) instability of a layer with non-linear viscosity and convective thinning of continental lithosphere, *Geophys. J. Int.*, *128*(1), 125–150, doi:10.1111/j.1365-246X.1997.tb04075.x.

Jagoutz, O., and M. D. Behn (2013), Foundering of lower island-arc crust as an explanation for the origin of the continental Moho, *Nature*, *504*(7478), 131–134.

Jaupart, C., and J. C. Mareschal (1999), The thermal structure and thickness of continental roots, *Dev. Geotectonics*, *24*, 93–114.

Jones, C. H., H. Kanamori, and S. W. Roecker (1994), Missing roots and mantle "drips": Regional Pn and teleseismic arrival times in the southern Sierra Nevada and vicinity, California, *J. Geophys. Res.*, *99*(B3), 4567–4601, doi:10.1029/93JB01232.

Jull, M., and P. B. Kelemen (2001), On the conditions for lower crustal convective instability, *J. Geophys. Res.*, *106*(B4), 6423–6446, doi:10.1029/2000JB900357.

Karato, S. I., and P. Wu (1993), Rheology of the upper mantle: A synthesis, *Science*, *260*(5109), 771–778.

Katz, R. F., M. Spiegelman, and C. H. Langmuir (2003), A new parameterization of hydrous mantle melting, *Geochem. Geophys. Geosyst.*, *4*(9), 1073, doi:10.1029/2002GC000433.

Kay, R. W., and S. M. Kay (1993), Delamination and delamination magmatism, *Tectonophysics*, *219*, 177–189.

Kay, S. M., B. Coira, and J. Viramonte (1994), Young mafic back-arc volcanic rocks as indicators of continental lithospheric delamination beneath the Argentine Puna Plateau, Central Andes, *J. Geophys. Res.*, *99*, 24,323–24,339, doi:10.1029/94JB00896.

Kay, S. M., B. Coira, G. Wörner, R. W. Kay, and B. S. Singer (2011), Geochemical, isotopic and single crystal ^{40}Ar/^{39}Ar age constraints on the evolution of the Cerro Galán ignimbrites, *Bull. Volcanol.*, *73*(10), 1487–1511.

Kear, D. (2004), Reassessment of Neogene tectonism and volcanism in North Island, New Zealand, *N. Z. J. Geol. Geophys.*, *47*(3), 361–374.

Krystopowicz, N. J., and C. A. Currie (2013), Crustal eclogitization and lithosphere delamination in orogens, *Earth Planet. Sci. Lett.*, *361*, 195–207.

Lambart, S., D. Laporte, and P. Schiano (2009), An experimental study of pyroxenite partial melts at 1 and 1.5 GPa: Implications for the major-element composition of Mid-Ocean Ridge Basalts, *Earth Planet. Sci. Lett.*, *288*(1), 335–347.

Lee, C. T. A., X. Cheng, and U. Horodyskyj (2006), The development and refinement of continental arcs by primary basaltic magmatism, garnet pyroxenite accumulation, basaltic recharge and delamination: Insights from the Sierra Nevada, California, *Contrib. Mineral. Petrol.*, *151*(2), 222–242.

Lee, C. T. A., P. Luffi, T. Plank, H. Dalton, and W. P. Leeman (2009), Constraints on the depths and temperatures of basaltic magma generation on Earth and other terrestrial planets using new thermobarometers for mafic magmas, *Earth Planet. Sci. Lett.*, *279*(1), 20–33.

Lee, C. T. A., P. Luffi, and E. J. Chin (2011), Building and destroying continental mantle, *Annu. Rev. Earth Planet. Sci.*, *39*, 59–90.

Lindsay, J. M., A. K. Schmitt, R. B. Trumbull, S. L. De Silva, W. Siebel, and R. Emmermann (2001), Magmatic evolution of the La Pacana caldera system, Central Andes, Chile: Compositional variation of two cogenetic, large-volume felsic ignimbrites, *J. Petrol.*, *42*(3), 459–486.

Manley, C. R., A. F. Glazner, and G. L. Farmer (2000), Timing of volcanism in the Sierra Nevada of California: Evidence for Pliocene delamination of the batholithic root?, *Geology*, *28*(9), 811–814.

Molnar, P., and G. A. Houseman (2004), The effects of buoyant crust on the gravitational instability of thickened mantle lithosphere at zones of intracontinental convergence, *Geophys. J. Int.*, *158*(3), 1134–1150, doi:10.1111/j.1365-246X.2004.02312.x.

Molnar, P., and G. A. Houseman (2013), Rayleigh-Taylor instability, lithospheric dynamics, surface topography at convergent mountain belts, and gravity anomalies, *J. Geophys. Res. Solid Earth*, *118*, 2544–2557, doi:10.1002/jgrb.50203.

Molnar, P., G. A. Houseman, and C. P. Conrad (1998), Rayleigh–Taylor instability and convective thinning of mechanically thickened lithosphere: Effects of non-linear viscosity decreasing exponentially with depth and of horizontal shortening of the layer, *Geophys. J. Int.*, *133*(3), 568–584.

Moore, J. G., and F. C. Dodge (1980), Late Cenozoic volcanic rocks of the southern Sierra Nevada, California: I. Geology and petrology: Summary, *Geol. Soc. Am. Bull.*, *91*(9), 515–518.

Morency, C., and M. P. Doin (2004), Numerical simulations of the mantle lithosphere delamination, *J. Geophys. Res.*, *109*, B03410, doi:10.1029/2003JB002414.

Murray, K. E., M. N. Ducea, and L. Schoenbohm (2015), Foundering-driven lithospheric melting: The source of central Andean mafic lavas on the Puna Plateau (22°S–27°S), *Geol. Soc. Am. Mem.*, *212*, 139–166.

Myers, S., S. Beck, G. Zandt, and T. Wallace (1998), Lithospheric-scale structure across the Bolivian Andes from tomographic images of velocity and attenuation for *P* and *S* waves, *J. Geophys. Res.*, *103*(21), 233–21,252.

Naimark, B. M., and A. T. Ismail-Zadeh (1995), Numerical models of a subsidence mechanism in intracratonic basins: Application to North American basins, *Geophys. J. Int.*, *123*(1), 149–160.

Nair, R., and T. Chacko (2008), Role of oceanic plateaus in the initiation of subduction and origin of continental crust, *Geology*, *36*(7), 583–586.

Neil, E. A., and G. A. Houseman (1999), Rayleigh-Taylor instability of the upper mantle and its role in intraplate orogeny, *Geophys. J. Int.*, *138*(1), 89–107, doi:10.1046/j.1365-246x.1999.00841.x.

Petermann, M., and M. M. Hirschmann (2003), Partial melting experiments on a MORB-like pyroxenite between 2 and 3 GPa: Constraints on the presence of pyroxenite in basalt source regions from solidus location and melting rate, *J. Geophys. Res.*, *108*(B2), 2125, doi:10.1029/2000JB000118.

Plank, T. (2005), Constraints from thorium/lanthanum on sediment recycling at subduction zones and the evolution of the continents, *J. Petrol.*, *46*(5), 921–944.

Putirka, K., and C. J. Busby (2007), The tectonic significance of high-K_2O volcanism in the Sierra Nevada, California, *Geology*, *35*(10), 923–926.

Pysklywec, R. N., and C. Beaumont (2004), Intraplate tectonics: feedback between radioactive thermal weakening and crustal deformation driven by mantle lithosphere instabilities, *Earth Planet. Sci. Lett.*, *221*(1), 275–292, doi:10.1016/S0012-821X(04)00098-6.

Rapp, R. P., and E. B. Watson (1995), Dehydration melting of metabasalt at 8–32 kbar: Implications for continental growth and crust-mantle recycling, *J. Petrol.*, *36*(4), 891–931.

Roy, M., T. H. Jordan, and J. Pederson (2009), Colorado Plateau magmatism and uplift by warming of heterogeneous lithosphere, *Nature*, *459*(7249), 978–982.

Rudnick, R. L., and D. M. Fountain (1995), Nature and composition of the continental crust: A lower crustal perspective, *Rev. Geophys.*, *33*(3), 267–309, doi:10.1029/95RG01302.

Saleeby, J., L. Le Pourhiet, Z. Saleeby, and M. Gurnis (2012), Epeirogenic transients related to mantle lithosphere removal in the southern Sierra Nevada region, California, part l: Implications of thermomechanical modeling, *Geosphere*, *8*(6), 1286–1309.

Saleeby, J., Z. Saleeby, and L. Le Pourhiet (2013), Epeirogenic transients related to mantle lithosphere removal in the southern Sierra Nevada region, California: Part II. Implications of rock uplift and basin subsidence relations, *Geosphere*, *9*(3), 394–425.

Salmon, M., B. L. N. Kennett, T. Stern, and A. R. A. Aitken (2013), The Moho in Australia and New Zealand, *Tectonophysics*, *609*, 288–298.

Schilling, F. R., et al. (2006), Partial melting in the Central Andean crust: A review of geophysical, petrophysical, and petrologic evidence, in *The Andes*, pp. 459–474, Springer, Berlin.

Schoenbohm, L. M., and B. Carrapa (2015), Miocene-Pliocene shortening, extension and mafic magmatism support small-scale lithospheric foundering in the central Andes, NW Argentina, in *Geodynamics of a Cordilleran Orogenic System: The Central Andes of Argentina and Northern Chile*, edited by P. G. DeCelles et al., *Mem. Geol. Soc. Am.*, *212*, MWR212-09, doi:10.1130/2015.1212(09).

Schurr, B., A. Rietbrock, G. Asch, R. Kind, and O. Oncken (2006), Evidence for lithospheric detachment in the central Andes from local earthquake tomography, *Tectonophysics*, *415*(1), 203–223, doi:10.1016/j.tecto.2005.12.007.

Springer, M. (1999), Interpretation of heat-flow density in the Central Andes, *Tectonophysics*, *306*(3), 377–395.

Stern, T., G. Houseman, M. Salmon, and L. Evans (2013), Instability of a lithospheric step beneath western North Island, New Zealand, *Geology*, *41*(4), 423–426.

Stern, T. A., W. R. Stratford, and M. L. Salmon (2006), Subduction evolution and mantle dynamics at a continental margin: Central North Island, New Zealand, *Rev. Geophys.*, *44*, RG4002, doi:10.1029/2005RG000171.

Thurner, S., I. Palomeras, A. Levander, R. Carbonell, and C. T. Lee (2014), Ongoing lithospheric removal in the western Mediterranean: Evidence from Ps receiver functions and thermobarometry of Neogene basalts (PICASSO project), *Geochem. Geophys. Geosyst.*, *15*, 1113–1127, doi:10.1002/2013GC005124.

Turcotte, D. L., and G. Schubert (2002), *Geodynamics*, Cambridge Univ. Press, New York.

Turner, S., C. Hawkesworth, J. Liu, N. Rogers, S. Kelley, and P. van Calsteren (1993), Timing of Tibetan uplift constrained by analysis of volcanic rocks, *Nature*, *364*(6432), 50–54.

Turner, S., N. Arnaud, J. Liu, N. Rogers, C. Hawkesworth, N. Harris, S. Kelley, P. Van Calsteren, and W. Deng (1996), Post-collision, shoshonitic volcanism on the Tibetan Plateau: Implications for convective thinning of the lithosphere and the source of ocean island basalts, *J. Petrol.*, *37*(1), 45–71.

Van Wijk, J. W., W. S. Baldridge, J. Van Hunen, S. Goes, R. Aster, D. D. Coblentz, S. P. Grand, and J. Ni (2010), Small-scale convection at the edge of the Colorado Plateau: Implications for topography, magmatism, and evolution of Proterozoic lithosphere, *Geology*, *38*(7), 611–614.

Wang, H. (2015), Intracontinental deformation caused by gravitational lithosphere removal, PhD thesis, Dep. of Phys., Univ. of Alberta, Edmonton, Alberta, Canada.

Wang, H., C. A. Currie, and P. G. DeCelles (2015), Hinterland basin formation and gravitational instabilities in the central Andes: Constraints from gravity data and geodynamic models, *Geol. Soc. Am. Mem.*, *212*, 387–406.

West, J. D., M. J. Fouch, J. B. Roth, and L. T. Elkins-Tanton (2009), Vertical mantle flow associated with a lithospheric drip beneath the Great Basin, *Nat. Geosci.*, *2*(6), 439–444.

Zandt, G., and C. R. Carrigan (1993), Small-scale convective instability and upper mantle viscosity under California, *Science*, *261*(5120), 460–463.